Basin Research

IAS EAGE

Basin Research (2015) **27**, 546–572, doi: 10.1111/bre.12088

Detrital thermochronologic record of burial heating and sediment recycling in the Magallanes foreland basin, Patagonian Andes

Julie C. Fosdick,* Marty Grove,† Stephan A. Graham,† Jeremy K. Hourigan,‡ Oscar Lovera§ and Brian W. Romans¶

*Geological Sciences, Indiana University, Bloomington, IN, USA
†Geological & Environmental Sciences, Stanford University, Stanford, CA, USA
‡Earth Sciences, University of California, Santa Cruz, CA, USA
§Earth & Space Sciences, University of California, Los Angeles, CA, USA
¶Geosciences, Virginia Polytechnic Institute and State University, Blacksburg, VA, USA

ABSTRACT

The Patagonian Magallanes retroarc foreland basin affords an excellent case study of sediment burial recycling within a thrust belt setting. We report combined detrital zircon U–Pb geochronology and (U–Th)/He thermochronology data and thermal modelling results that confirm delivery of both rapidly cooled, first-cycle volcanogenic sediments from the Patagonian magmatic arc and recycled sediment from deeply buried and exhumed Cretaceous foredeep strata to the Cenozoic depocentre of the Patagonian Magallanes basin. We have quantified the magnitude of Eocene heating with thermal models that simultaneously forward model detrital zircon (U–Th)/He dates for best-fit thermal histories. Our results indicate that 54–45 Ma burial of the Maastrichtian Dorotea Formation produced 164–180 °C conditions and heating to within the zircon He partial retention zone. Such deep burial is unusual for Andean foreland basins and may have resulted from combined effects of high basal heat flow and high sediment accumulation within a rapidly subsiding foredeep that was floored by basement weakened by previous Late Jurassic rifting. In this interpretation, Cenozoic thrust-related deformation deeply eroded the Dorotea Formation from *ca.* 5 km burial depths and may be responsible for the development of a basin-wide Palaeogene unconformity. Results from the Cenozoic Río Turbio and Santa Cruz formations confirm that they contain both Cenozoic first-cycle zircon from the Patagonian magmatic arc and highly outgassed zircon recycled from older basin strata that experienced burial histories similar to those of the Dorotea Formation.

INTRODUCTION

Sedimentary basins chronicle the erosional history of their sediment sources, offering invaluable information about orogenic unroofing histories and inferred deformational events in diverse tectonic environments (e.g. Dickinson & Suczek, 1979; Steidtmann & Schmitt, 1988). Integration of complementary sedimentary provenance methods including conglomerate and sandstone petrography, palaeocurrent measurements, geochemical analysis and detrital zircon geochronology can provide powerful fingerprinting of source regions (e.g. Suttner, 1974; Graham *et al.*, 1986; Dickinson, 1988; Heller and Frost, 1988; Degraaff-Surpless *et al.*, 2002). In tectonically complex environments such as thrust belts, however, more information is often required to recognize sediment recycling of lithologic units and older thrust belt cannibalization that can lead to ambiguous sedimentary provenance interpretations. Such factors are critical for assessing long-term sediment budgets, interactions between tectonics and sedimentation, nutrient flux from the continents into the deep sea and the distribution of natural resources.

Sediment recycling is expected in many tectonic settings, such as foreland basins, where the path followed by grains initially derived from erosion of a basement source region typically involves significant intermediate stages of crustal evolution before the detritus is finally incorporated into tectonically stable basin strata. Figure 1 illustrates how sediments eroded from the active thrust belt may be tectonically buried beneath advancing thrusts and sedimentary overburden and later re-exhumed by thrusting to serve as the source terrane for younger sedimentary rocks in the basin (e.g. Schmitt & Steidtmann, 1990; Graham *et al.*, 1993). The shallow crustal histories experienced by eroded sediment are associated with important differences in thermal histories (Fig. 1) that go undetected by traditional provenance methods, but are potentially recoverable by thermochronologic methods.

Correspondence: Julie C. Fosdick, Department of Geological Sciences, Indiana University, Bloomington, IN 47404, USA. E-mail: jfosdick@indiana.edu

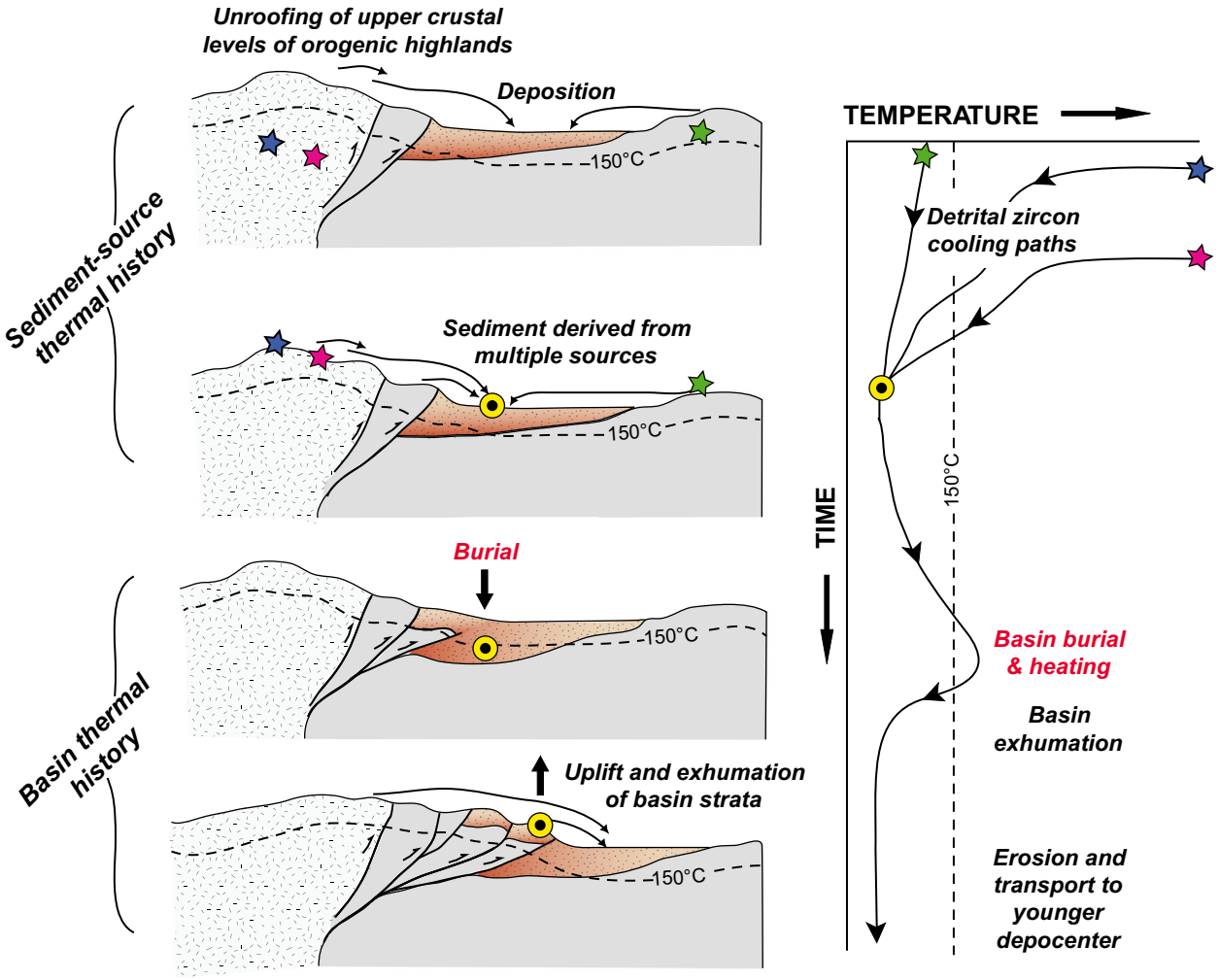

Fig. 1. Schematic illustration of sediment source terranes and basinfill in a typical foreland basin setting showing the thermal evolution of sediment during its detrital exhumation history (upper panels) and its subsequent basin thermal history (lower panels).

The Patagonian Magallanes retroarc foreland basin of southern South America (Fig. 2) provides an excellent geologic setting to explore complex sediment and source thermal histories via combined zircon U–Pb and He age dating. Many stratigraphic and provenance studies have focused upon the Upper Cretaceous Patagonian Magallanes basin strata (e.g. Katz, 1963; Macellari *et al.*, 1989; Biddle *et al.*, 1986; Wilson, 1991; Fildani *et al.*, 2003; Fildani & Hessler, 2005; Romans *et al.*, 2010; Bernhardt *et al.*, 2011; McAtamney *et al.*, 2011) that have demonstrated sustained sedimentary connectivity between the southern Patagonian batholith (Hervé *et al.*, 2007b) and the age-equivalent thrust belt and marine foredeep in the Patagonian Andes. Throughout the Late Cretaceous, sediment dispersal systems provided a remarkably continuous supply of batholith-sourced zircon to the basin (Fig. 2). Recent work on the Palaeogene nonmarine basinfill also records a prominent arc source during early Cenozoic Patagonian foreland basin evolution at this latitude (Otero *et al.*, 2012; Schwartz *et al.*, 2012). However, the detailed path taken by this batholith-derived detritus remains unclear. Because of the tectonic activity of the thrust belt throughout the latest Cretaceous and early Cenozoic, it is likely that foreland basin sediment – also batholith-derived – of this age experienced protracted latest Cretaceous – early Cenozoic burial. Continued thrust deformation ultimately exhumed and eroded these strata and reworked the detritus into younger Cenozoic deposits. In some cases, Cenozoic thrust burial of Upper Cretaceous strata occurred to depths sufficient to partially degas He from zircon (Fosdick *et al.*, 2013).

Thermochronology relies upon the balance of radiogenic ingrowth and thermally activated diffusive loss of daughter products of radioactive decay in minerals and thus provides a sensitive tool for constraining temperature–time histories. Detrital thermochronology methods such as $^{40}Ar/^{39}Ar$ in muscovite and K-feldspar, and fission track and (U–Th)/He analysis of apatite and zircon have been widely exploited to elucidate the thermal histories of sedimentary basins and their respective source regions (Reiners & Brandon, 2006). Combined dating of two or more chronologic systems with differing temperature sensitivity in the same phase can significantly increase the ability to interpret detrital thermochronology

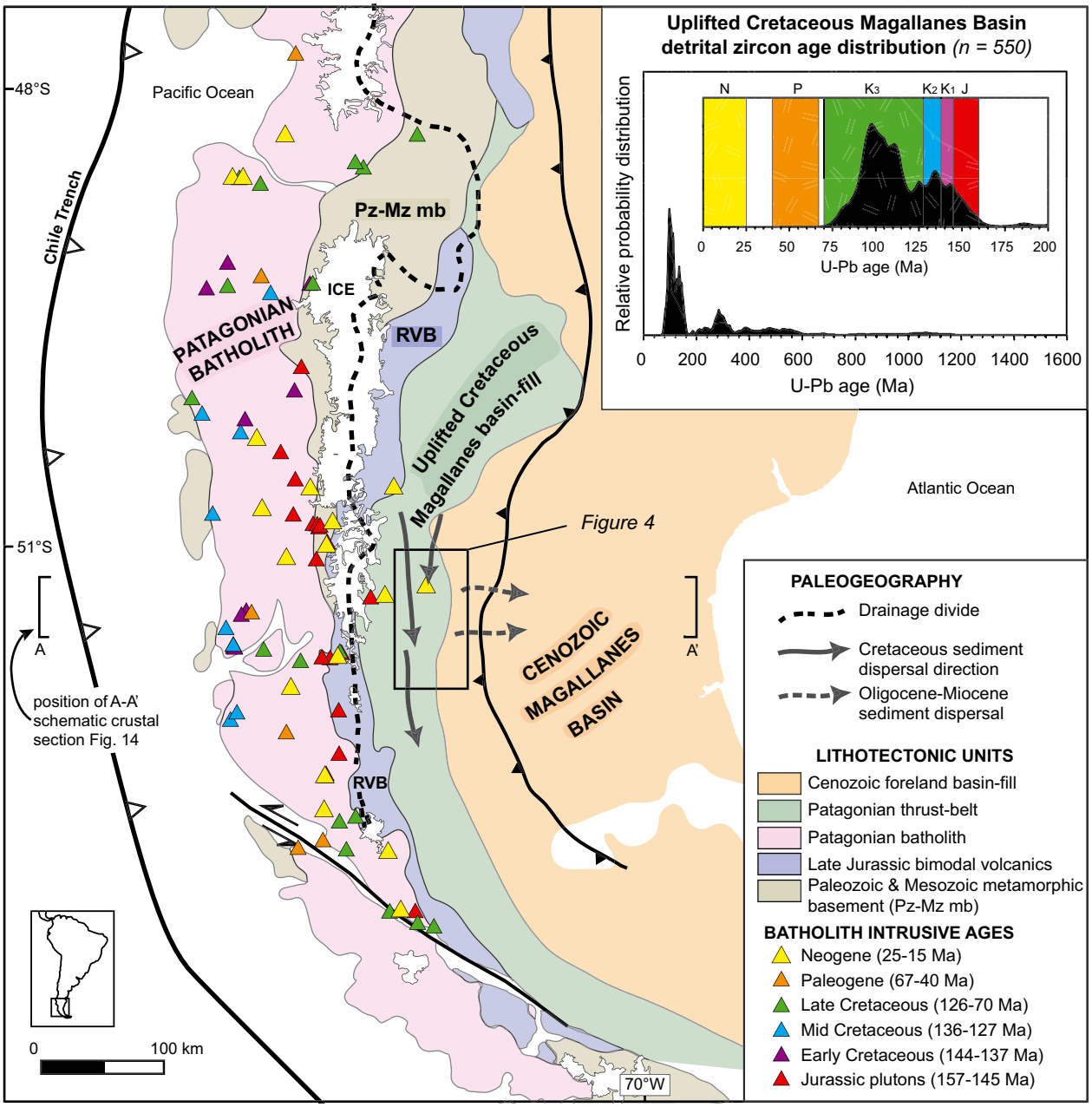

Fig. 2. Tectonostratigraphic map of the southern Patagonian Andes showing the location of the study area (Fig. 4). Triangles show pluton ages of the Patagonian batholith, a major sediment source to the foreland basin (intrusive intervals defined by Hervé *et al.*, 2007b). Grey arrows indicate general sediment dispersal patterns for the Late Cretaceous basin (solid) and Oligocene–Miocene basin (dashed). Inset: compiled detrital U–Pb age distributions from the Patagonian Cretaceous Magallanes basin (compiled from Fildani *et al.*, 2003; Romans *et al.*, 2010; Bernhardt *et al.*, 2011) in comparison to the batholith intrusive ages (shown by coloured panels).

results. Consequently, U–Pb and He double dating of zircon has been increasingly exploited in provenance studies to extract complementary crystallization age and thermal history information from the same detrital grains to better assess source region characterization (e.g. Rahl *et al.*, 2003; Reiners *et al.*, 2005; Saylor *et al.*, 2012). The ability to quantitatively constrain basin heating requires careful integration of complementary approaches such as combined U–Pb and He dating of detrital zircons (e.g. Reiners *et al.*, 2005) with other geologic constraints. Analysing such data with numerical models that fully explore parameter space (e.g. Lovera *et al.*, 1999; Ketcham, 2005; Guenthner *et al.*, 2013) allows otherwise unobtainable estimates of the magnitude and duration of dynamic processes in active tectonic settings such as thrust belts.

In this study, we have measured combined detrital zircon U–Pb and He ages from the Maastrichtian through Middle Miocene Magallanes basin sediments to address the following questions: (1) How significant was foreland basin burial heating during Cenozoic advancement of

thrust deformation? (2) Can we differentiate between sediment derived directly from the magmatic arc vs. reworked Cretaceous deposits exposed in the thrust belt? (3) How has growth of the Patagonian thrust belt altered Cenozoic sediment dispersal patterns? Answers to these questions not only improve our understanding of Patagonian foreland basin evolution but also provide valuable insight into the broader interactions between tectonics and sedimentation, basin thermal histories, and signals of sediment recycling in convergent basins.

Our study initially focuses upon the thermal history of detritus from deeply buried Maastrichtian deposits whose He age systematics primarily record foreland basin heating. We then examine the Middle Miocene sediments that appear to have received first-cycle sediment input both directly from magmatic arc sources and indirectly as recycled detritus eroded from deeply buried and exhumed Upper Cretaceous strata. Our analysis includes development of a forward modelling approach to systematically explore a wide range of temperature–time histories of zircon to deduce the family of conditions capable of reproducing the measured U–Pb and He age distributions. We first modelled our detrital zircon results individually and then collectively to test the hypothesis that grains share a common thermal history. Simultaneous modelling of all grains in the age distribution was assessed statistically. Although our models emphasize common basin heating histories, they are constructed in such a manner that they are also capable of crudely simulating the earlier thermal history of original source region. This novel modelling approach has allowed us to resolve first-cycle sedimentation from sediment recycling involving post-depositional burial heating and should be applicable to thrust belt settings and similar environments elsewhere.

GEOLOGIC SETTING AND PREVIOUS WORK

The Magallanes foreland basin is one of the thickest sedimentary accumulations known within the South American continent and provides an excellent record of Andean orogenesis since Late Cretaceous time (Katz, 1963; Natland *et al.*, 1974; Biddle *et al.*, 1986; Wilson, 1991; Fildani & Hessler, 2005). The character of the basin is partly a function of tectonic inheritance. Subduction-related processes, beginning with Gondwanan orogenic events, have affected the western margin of South America since Cambrian time (Pankhurst *et al.*, 2006). Conversely, crustal extension related to the initial break-up of southern Gondwana and eastward drift of Africa away from South America formed a marginal oceanic basin, the Rocas Verdes Basin in the Patagonian region in the latest Jurassic Period (Katz, 1963; Dalziel *et al.*, 1974). Extension across the Rocas Verdes Basin culminated in the formation of quasi-oceanic and attenuated crust characterized by ophiolitic assemblages and bimodal volcanism located east of the Jurassic arc (Allen, 1982; Calderón *et al.*, 2007). Closure and basin inversion of the northern Rocas Verdes Basin that began in Early Cretaceous time (Dalziel *et al.*, 1974; Wilson, 1991; Fildani & Hessler, 2005) culminated in Late Cretaceous development of the east-directed Patagonian thrust belt (Fig. 2) (Wilson, 1991; Kraemer, 1998; Fosdick *et al.*, 2011a).

Southern Patagonian batholith

The southern Patagonian batholith was emplaced into predominately Palaeozoic metasedimentary wallrocks that exhibit a broad range of Mesoproterozoic to early Mesozoic zircon U–Pb ages with prominent clusters occurring between 250–300, 550–600 and 950–1150 Ma (Forsythe & Allen, 1980; Hervé *et al.*, 2003; Pankhurst *et al.*, 2006). The southern Patagonian batholith itself was constructed in six major intrusive phases since Late Jurassic time (Hervé *et al.*, 2007b), although initial magmatism overlapped in time with intraplate magmatism associated with Gondwana break-up (Pankhurst *et al.*, 2000). Middle Jurassic magmatism and generation of bimodal volcanics that overlapped with the time of rifting of the southern Atlantic Ocean was focused mostly in the east (Pankhurst *et al.*, 2000). Subsequent Late Jurassic to Middle Cretaceous calc-alkaline arc magmatism was established near the western continental margin (Fig. 2). Since Late Cretaceous time, arc magmatism has generally migrated eastward across the orogen (Ramírez de Arellano *et al.*, 2012), giving rise to a belt of Palaeogene plutons emplaced along the axis of the composite Mesozoic batholith. Subsequent Neogene subduction-related calc-alkaline and slab-window magmatism of ocean island basalt affinity was distributed over a broader region including positions farther east into rocks of the foreland basin (Fig. 2) (Hervé *et al.*, 2007b; Ramírez de Arellano *et al.*, 2012).

Tectonic controls upon depositional patterns in the Magallanes basin

Thrust loading of dense oceanic and attenuated continental crust along the eastern margin of the Late Jurassic–Cretaceous Patagonia batholith produced a deep axial depression that became the Magallanes foreland basin (e.g. Natland *et al.*, 1974; Wilson, 1991; Fildani & Hessler, 2005; Romans *et al.*, 2011). Detrital zircon results from the Upper Cretaceous Patagonian Magallanes basin, summarized in the inset to Fig. 2 (Fildani *et al.*, 2003; Romans *et al.*, 2010), agree with other geologic evidence that collectively indicate that the Late Jurassic through Neogene plutons of the Patagonian batholith were the primary contributor of sediment to the Patagonian Magallanes basin throughout its history at this latitude (Forsythe & Allen, 1980; Hervé *et al.*, 2003; Pankhurst *et al.*, 2003; Fildani *et al.*, 2003; Hervé *et al.* (2004); Romans *et al.*, 2011; Bernhardt *et al.*, 2011). Sandstone petrography and mudstone geochemistry of turbidites of the Turonian Punta Barrosa Formation deposited in the incipient foreland basin also indicate that subordinate

amounts of sediment was sourced from local basement highs represented by the Rocas Verdes Basin, Palaeozoic to earliest Mesozoic metamorphic basement complexes, and the Sarmiento ophiolitic complex (Fildani & Hessler, 2005).

Southward-directed deposition

Palaeocurrent data from many studies establish a south-directed sediment dispersal system, reflecting an axial basin configuration that persisted for *ca.* 20 Myr during the Late Cretaceous (e.g. Katz, 1963; Scott, 1966; Winn & Dott, 1979; Fildani & Hessler, 2005; Crane & Lowe, 2008; Hubbard *et al.*, 2008; Armitage *et al.*, 2009; Covault *et al.*, 2009). As the Patagonian thrust belt widened and propagated eastward, erosion of uplifted Upper Jurassic volcanic rocks of the Rocas Verdes Basin and Jurassic–Cretaceous granitoids of the Patagonia batholith provided detritus to Coniacian strata (*ca.* 88 Ma) of the northern Magallanes basin (Romans *et al.*, 2010). In addition, abundant metamorphosed rhyolite clasts derived from the Tobífera Formation appeared in the basinfill at this time. Overall, zircon age distributions and sandstone petrography varied little during Late Cretaceous basin evolution, with the bulk of sediments shed from the batholith and lesser components derived from metamorphic basement and ophiolitic complexes.

Cenozoic basin configuration

A major shift in sediment dispersal patterns within the Patagonian Magallanes basin occurred during the early Cenozoic Era. By Palaeogene time, the deformational front of the thrust belt had migrated *ca.* 40 km eastward across the foreland (Fosdick *et al.*, 2011a). Thrust faults shortened and uplifted the Cretaceous depocentre, displacing the Eocene through Miocene shallow marine and fluvial-deltaic foredeep eastward (Fig. 2) (Dalziel, 1986; Wilson, 1991; Malumián *et al.*, 2000; Fosdick *et al.*, 2011a). Subsurface imaging of the sedimentary infill characterizes dominantly northeast-directed prograding clinoforms within Lower Eocene through Oligocene strata (Biddle *et al.*, 1986). Palaeocurrent indicators measured from outcrops depict a locally more complicated picture during Cenozoic basin history. Eocene and Oligocene coastal plain and deltaic sedimentation suggest more northwesterly sediment transport (Le Roux *et al.*, 2010; Pearson *et al.*, 2012), possibly indicative of backbulge-derived sediments transported westward into the foredeep (Schwartz *et al.*, 2012). Fluvial systems developed in Early to Middle Miocene time document eastward transport of coarse sediments that were shed off of the thrust belt (Malumián *et al.*, 2000).

Source region thermal history

The early Cenozoic tectonic deformation and uplift of the Upper Cretaceous depocentre introduced an important new source of detritus into the Magallanes basin: recycled Late Jurassic through Cretaceous arc-derived detritus from these uplifted Cretaceous basin strata. Thermochronology data from more deeply buried stratigraphy within the interior of the thrust belt record burial temperatures that exceeded *ca.* 190 °C (Fosdick *et al.*, 2013). Whole rock K–Ar and phengite $^{40}Ar/^{39}Ar$ cooling ages between 80 and 70 Ma from the Late Jurassic Tobífera Formation have also been interpreted to record regional exhumation of the Tobífera metavolcanic rocks through 350 °C (Galaz *et al.*, 2005; Hervé *et al.*, 2007a; Calderón *et al.*, 2012).

Beginning in Oligocene time, the locus of exhumation shifted eastwards across the batholith (Thomson *et al.*, 2001) and the Patagonian thrust belt (Fosdick *et al.*, 2013). Available apatite fission-track data indicate that significantly less exhumation and erosion occurred within the Patagonia batholith relative to the thrust belt during this time. Figure 3 shows the distribution of apatite fission-track cooling ages from the batholith and Palaeozoic basement (Thomson *et al.*, 2001, 2010), and zircon He ages from the Andean thrust belt (Fosdick *et al.*, 2013). The oldest apatite fission-track ages are Palaeocene and Maastrichtian and come from rocks that are located along the westernmost parts of the orogenic belt, where Early Cretaceous plutons intrude Palaeozoic metamorphic wallrocks (Fig. 3) (Thomson *et al.*, 2001, 2010). The majority of the batholith records Miocene apatite fission-track ages (Fig. 3).

STRATIGRAPHIC CONTEXT OF CENOZOIC SAMPLE SUITE

Sampling for detrital thermochronology was performed from two areas within the Maastrichtian through Middle Miocene Magallanes basin to compare along-strike changes in sedimentary provenance and thermal history (Fig. 4). The Río Baguales and Cordillera Chica stratigraphic sections (Fig. 5) are separated by *ca.* 80 km along the east-dipping frontal monocline of the Patagonian thrust belt (Fig. 4). Three samples were selected from the Cordillera Chica section, whereas two samples were obtained from the Río Baguales section (Fig. 5).

Stratigraphic and biostratigraphic studies of the Upper Cretaceous–Middle Miocene foreland basin strata have established dominantly shallow marine, deltaic, and fluvial depositional environments (Natland *et al.*, 1974; Riccardi & Rolleri, 1980; Macellari *et al.*, 1989; Le Roux *et al.*, 2010). The regional distribution of these deposits spans national borders and local provinces, leading to numerous stratigraphic names for lithologically similar formations. We follow the stratigraphic subdivisions of Malumián *et al.* (2000) with revisions from the proposed stratigraphic nomenclature of Bostelmann *et al.* (2013).

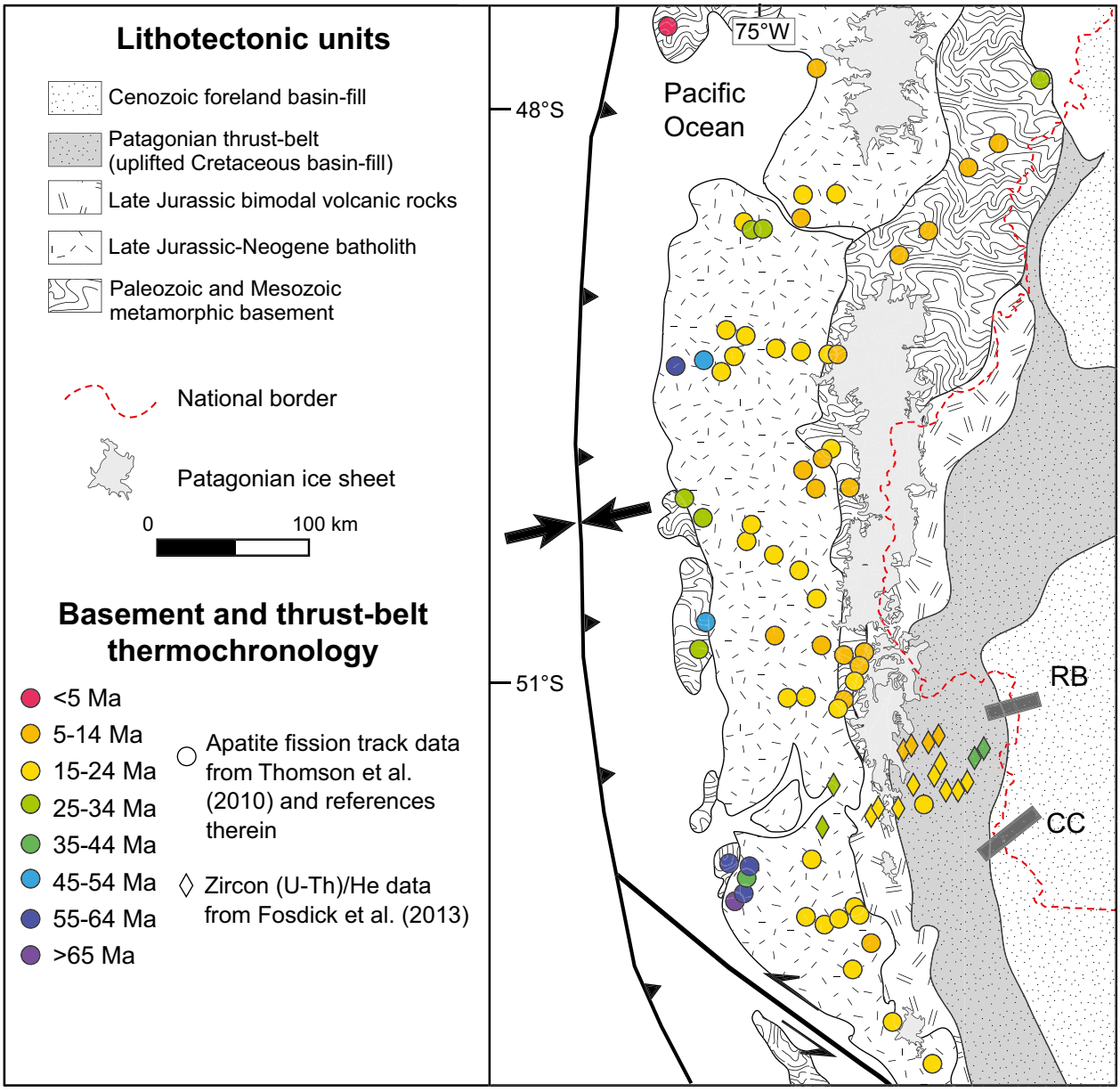

Fig. 3. Distribution of published basement and thrust belt thermochronology data from the Patagonian Andes. Apatite fission-track data (circles) are compiled from Thomson *et al.* (2010) and references therein. Zircon (U–Th)/He dates (diamonds) from the Patagonian thrust belt are from Fosdick *et al.* (2013). Both data sets show a general eastward younging of thermochronometer ages. Sampled stratigraphic sections are indicated by black bars and refer to the Río Baguales (RB) and Cordillera Chica (CC) sections.

Maastrichtian – Lower Palaeocene Dorotea Formation

The stratigraphically lowest sandstone samples were collected from the top of the Maastrichtian Dorotea Formation, which consists of deltaic sandstone deposited in a southward progradational axial foreland basin (Katz, 1963; Covault *et al.*, 2009; Romans *et al.*, 2009; Hubbard *et al.*, 2008; Schwartz *et al.*, 2012). This formation crops out along the Chile–Argentina border (Fig. 4), and correlates to the upper part of Cerro Cazador and overlying Dorotea formations in Argentina (Fig. 5) (Hünicken, 1955; Malumián & Caramés, 1997). To the north near Lago Argentino, the Dorotea Formation transitions laterally to shoreface and lagoonal facies (Riccardi & Rolleri, 1980). The depositional age of the Dorotea Formation is well-established as Maastrichtian, although the uppermost section is debated due in part to differences in stratigraphic preservation from place to place. However, vertebrate fossils from the Río Baguales area suggest a Maastrichtian age (Riccardi & Rolleri, 1980; Macellari *et al.*, 1989), farther south in the Cerro Castillo area, the youngest strata could be Palaeocene, based on a Danian foraminiferal assemblage (Malumián & Caramés, 1997). For the Cordillera Chica stratigraphy (Fig. 4), detrital zircon U–Pb ages establish a Maastrichtian (*ca.* 72–68 Ma) maximum depositional age of the Dorotea Formation (Romans *et al.*, 2010; this study) (Fig. 5).

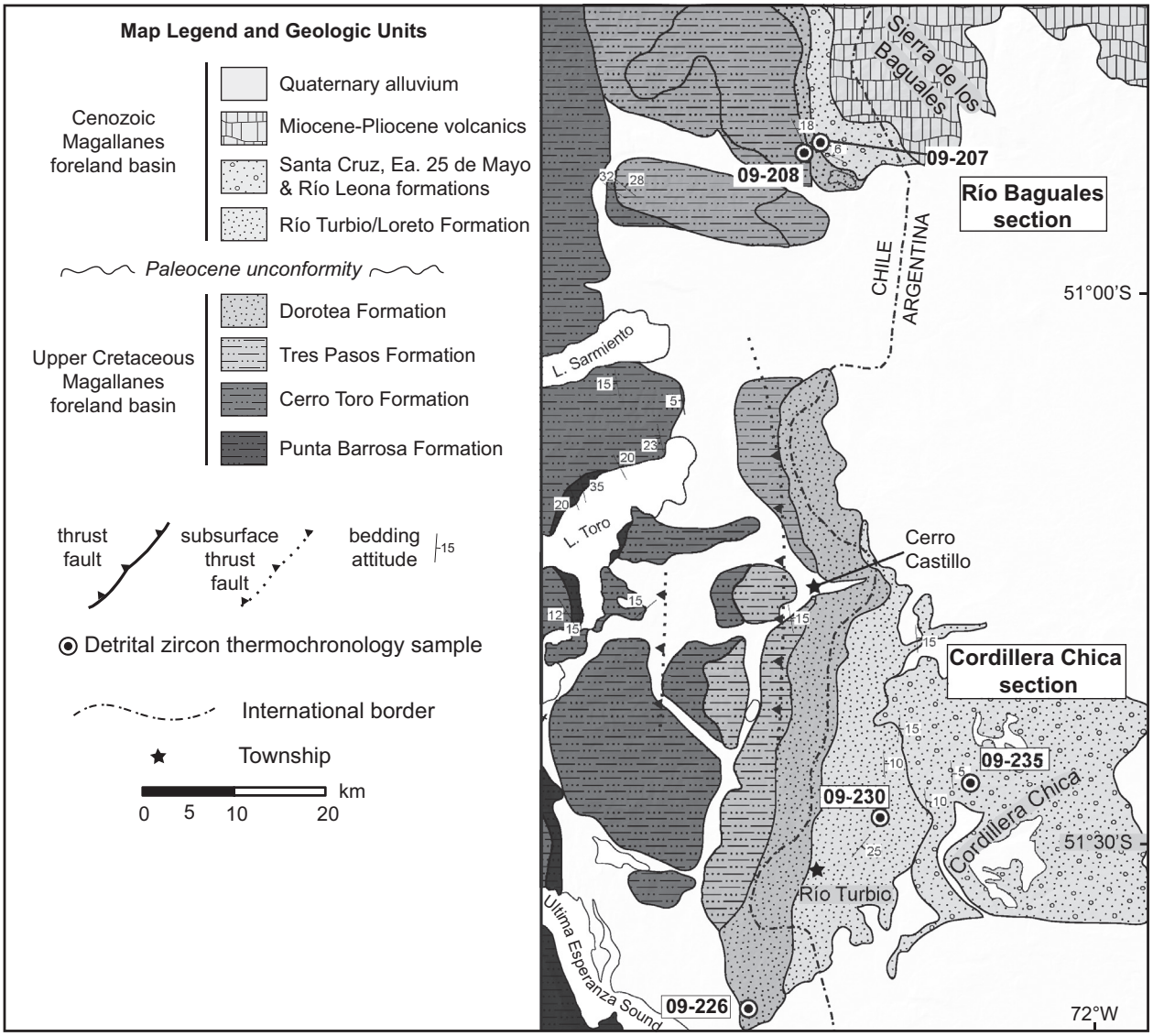

Fig. 4. Sample localities for detrital zircon geochronology and thermochronology. The Río Baguales and Cordillera Chica study areas are located along the eastern margin of the Patagonian thrust belt in Chile and Argentina between 50°30'S and 51°40'S, where Cenozoic foreland basin strata are uplifted into an east-dipping monocline. Geology modified after Wilson (1983), Malumián *et al.* (2001), and Fosdick *et al.*, (2011a).

The Dorotea Formation is separated from Middle Eocene and younger strata by a significant unconformity (Fig. 5), resulting in a wedge-shaped formational geometry that thins towards the east and the north (Hünicken, 1955; Biddle *et al.*, 1986; Malumián *et al.*, 2000; Schwartz *et al.*, 2012). The geologic significance of this regional unconformity is debated. Early workers supported a gradational depositional contact with little missing time (Hünicken, 1955; Yrigoyen, 1969; Nullo *et al.*, 1981). More recent subsurface stratigraphic mapping, biostratigraphic and chronostratigraphic studies document a regionally extensive erosional surface and suggest *ca.* 30 Myr of missing Upper Palaeocene through Middle Eocene record (Biddle *et al.*, 1986; Malumián & Náñez, 1988; Malumián *et al.*, 2000; Schwartz *et al.*, 2012). Elsewhere in the Magallanes Basin, reported Palaeocene strata are restricted to Tierra del Fuego (Malumián and Caramés, 1997).The regional foreland unconformity has been interpreted to have been produced by an episode of crustal shortening and associated foreland uplift in relation to propagation of the thrust front (Malumián *et al.*, 2000).

Upper Eocene through Upper Oligocene stratigraphy

In the Cordillera Chica area, the Dorotea Formation is unconformably overlain by the Eocene–Oligocene (?) Río Turbio Formation, which is characterized by a shallow marine and lagoonal cobble conglomerate, sandstone and siltstone interbedded with glauconitic intervals, claystone and coquinas (Fig. 5) (Hünicken,

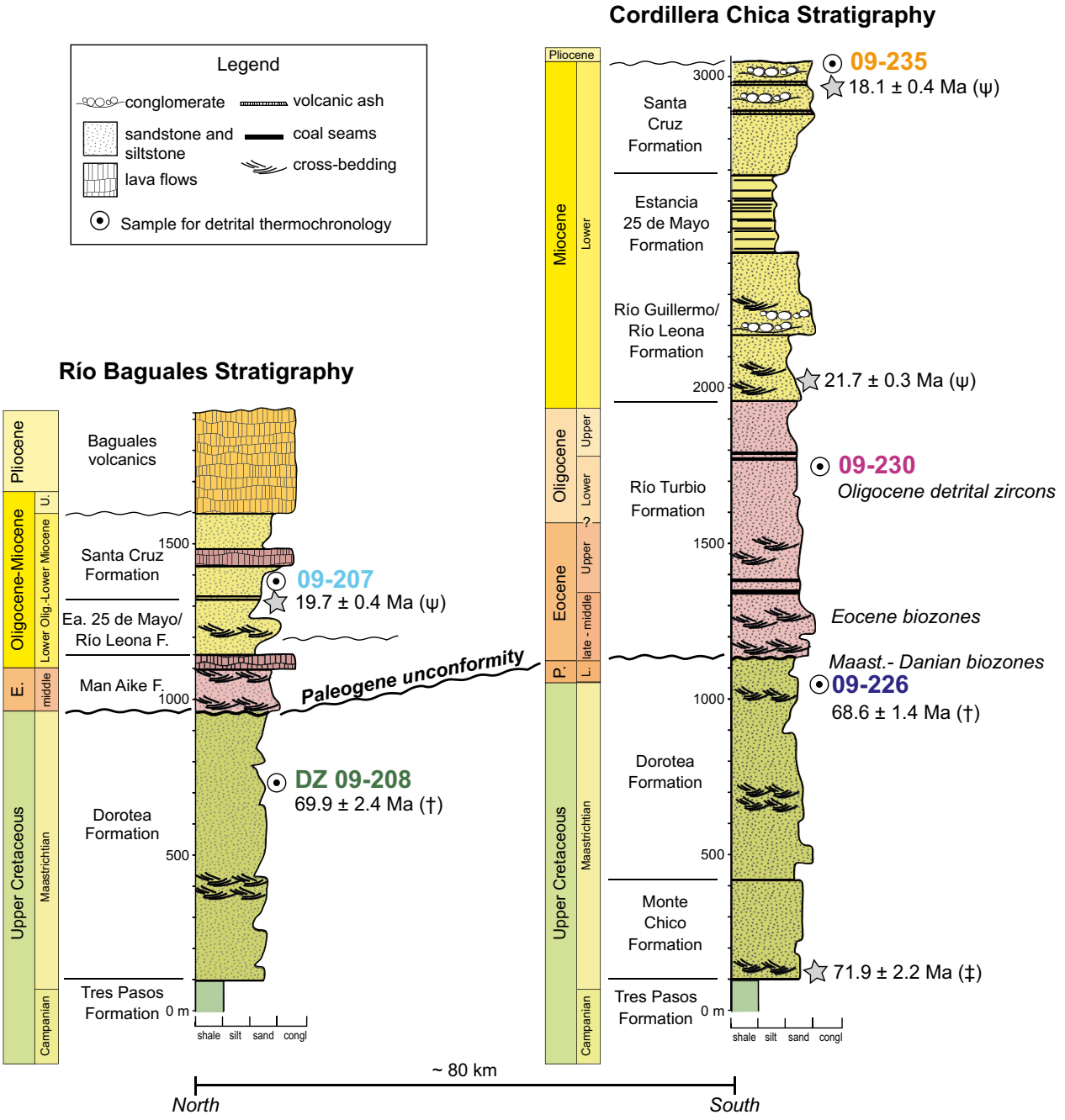

Fig. 5. Generalized stratigraphy and geochronology for the Río Baguales (north) and Cordillera Chica (south) study areas, following the stratigraphic nomenclature of Bostelmann *et al.* (2013). Stratigraphy of the Cordillera Chica composite section is simplified from Malumián & Caramés (1997) and Malumián *et al.* (2000). Stratigraphy of the Río Baguales section based on this work and Le Roux *et al.* (2010). White bull's-eyes show locations of detrital zircon thermochronology samples used in this study. Radiometric dates (grey stars) are eruptive ages of interbedded volcanic ash and lava flows (ψ after Fosdick *et al.*, 2011a), and maximum depositional ages measured from the youngest detrital zircon U–Pb age populations († this study; ‡ after Romans *et al.*, 2010). Depositional ages are based on these dates and microfaunal assemblages (see text for references).

1955; Malumián & Caramés, 1997; Pearson *et al.*, 2012). Thick and mineable coal seams are also a distinct component of the Río Turbio Formation in the Cordillera Chica area. Based on similar depositional age and general lithostratigraphy, this formation has been correlated regionally to the Man Aike Formation in the north (Furque, 1973; Casadío *et al.*, 2009) and to the Loreto Formation in the south (Hofftstetter *et al.*, 1957; Otero *et al.*, 2012). Early biostratigraphic studies suggested that deposition of the Loreto/Río Turbio formations spanned from the Palaeocene–Eocene at its base to Miocene at its top (Yrigoyen, 1969; Riccardi & Rolleri, 1980; Russo *et al.*, 1980). More recent studies have alternatively indicated a more restricted Eocene age for

the entire formation (Malumián & Caramés, 1997; Otero *et al.*, 2012). In particular, vertebrate palaeontology, botany and radiometric data sets from the Loreto Formation have supported an Upper Eocene age (Otero *et al.*, 2012). Additional detrital zircon U–Pb dating of the lower Man Aike Formation corroborate a Upper Eocene maximum depositional age (*ca.* 36–40 Ma) in the Río Baguales area (Le Roux *et al.*, 2010; Schwartz *et al.*, 2012). We collected one sandstone sample from the upper Río Turbio Formation (Fig. 5).

Eocene through Middle Miocene stratigraphy

The Río Turbio Formation is overlain by the nonmarine Río Guillermo and Río Leona formations, which consist of fluvial and coastal plain conglomerate, sandstone, coaly claystone and abundant silicified tree trunks (Fig. 5) (Malumián & Caramés, 1997). Riccardi & Rolleri (1980) assigned an Oligocene–Miocene age to the Río Guillermo Formation, and equated it with similar units across this stratigraphic interval of the Magallanes basin. An interbedded volcanic tuff collected from the upper Río Guillermo Formation yields a zircon U–Pb age of 21.7 ± 0.3 Ma (Fosdick *et al.*, 2011a). This Middle Miocene radiometric constraint on depositional age is consistent with the growing consensus derived from palaeontological assemblages (Bostelmann *et al.*, 2013).

The Early Miocene marine transgression across Patagonia resulted in widespread deposition of shallow marine and estuarine strata of the Estancia 25 de Mayo Formation (Cuitiño & Scasso, 2010). This unit is characterized by mudstone, sandstone, interbedded volcanic ash and abundant oyster fossils and plant remains. Radiometric studies from the Estancia 25 de Mayo Formation constrain deposition age between *ca.* 21 and 19 Ma (Cuitiño *et al.*, 2012). This unit grades upward and laterally into the Middle Miocene continental Santa Cruz Formation, which includes fluvial claystone, sandstone, conglomerate, volcanic tuff and a diverse faunal assemblage assigned to the Middle Miocene Santacrucian South American Land Mammal Ages interval (Malumián *et al.*, 1999; Bostelmann *et al.*, 2013). In the type-locality near Lago Argentino, the 22–14 Ma age of the Santa Cruz Formation is well-constrained by $^{40}Ar/^{39}Ar$ geochronology and represents the youngest preglacial basinfill preserved in the Magallanes basin (Blisniuk *et al.*, 2005). In the Cordillera Chica study area, zircon U–Pb geochronology from interbedded volcanic ash collected from the top of the Santa Cruz Formation yields a *ca.* 18.1 Ma ± 0.4 eruptive age (Fosdick *et al.*, 2011a) (Fig. 5).

METHODS

Detrital zircon U–Pb geochronology

Zircon extractions were carried out using standard crushing and sizing procedures following the methods in Fildani *et al.* (2003). Final zircon concentrates were inspected under a binocular microscope to remove obvious contaminants, mounted on tape in epoxy resin, and only lightly polished to maximize grain preservation for subsequent He analysis. U–Pb detrital zircon geochronology was conducted by LA-ICP-MS analysis at the LaserChron Center at the University of Arizona following the procedures outlined in Gehrels *et al.* (2006). Detrital zircons were randomly analysed from a linear swath of grains across the sample mount to minimize sampling bias in characterizing all detrital populations. Interpreted U–Pb ages use the ^{204}Pb corrected $^{206}Pb/^{238}U$ ratio for <1.0 Ga grains and the ^{204}Pb corrected $^{206}Pb/^{207}Pb$ ratio for >1.0 Ga grains. Analyses that were >30% normally discordant or >5% reverse discordant were excluded from interpretations. Analytical results are reported in the Supporting Information.

Detrital zircon He thermochronology

Zircon He thermochronology is based upon retention of alpha particles (^4He nuclei) produced during the decay of radioactive ^{238}U, ^{235}U and ^{232}Th. At high temperatures, ^4He diffusivities are sufficiently high that helium cannot be quantitatively retained in the U- and Th host phase (Zeitler *et al.*, 1987; Wolf *et al.*, 1996; Farley, 2002). As rocks cool towards the Earth's surface, He diffusivity also declines until diffusion is sufficiently sluggish that ^{4} He produced by U- and Th decay is quantitatively retained. The temperature range over which this transition occurs is termed the partial retention zone (PRZ) and nominally corresponds to *ca.* 200–160 °C for ^4He in zircon (Reiners *et al.*, 2004; Hourigan *et al.*, 2005), and perhaps as low as *ca.* 140 °C for zircons affected by radiation damage (e.g. Guenthner *et al.*, 2013). Robust thermochronologic interpretations of He dates require accurate characterization of zircon He diffusion kinetics, which can be affected by factors such as grain size, crystallography, anisotropic variations in He diffusion and radiation damage (e.g. Reiners, 2005; Cherniak *et al.*, 2009; Guenthner *et al.*, 2013; Ketcham *et al.*, 2013). The effective uranium concentration eU serves as a useful proxy for radiation damage (where eU = U + 0.235 x Th). As such, positive or negative He date-eU correlations can provide further constraints on a sample's thermal history.

Zircon He analyses were performed in the (U–Th)/He thermochronology laboratory at the University of California in Santa Cruz on a subset of detrital zircons for which U–Pb ages had already been determined. The lightly sectioned and polished grains were extracted from epoxy mounts, characterized, and encapsulated in Nb tubes. We selected between 17 and 26 grains per sample, targeting the major U–Pb populations with emphasis on youngest grains and the Cretaceous and Jurassic populations. This approach allowed us to directly compare He dates and U–Pb crystallization ages for representative populations. Complete gas extraction, mineral digestion procedures and analytical data are reported in the Supporting Information.

RESULTS

Detrital zircon U–Pb ages are shown in Fig. 6 as probability plots and corresponding histograms for the five sampled horizons in ascending stratigraphic order. The combined U–Pb and He results shown in Fig. 7 are presented in the same stratigraphic order. Each panel shows the U–Pb probability distributions on the *x*-axis for reference. The green bars in Fig. 7 represent the acceptable range in depositional age, based on available sources of data including biostratigraphy and the geochronology of interbedded volcanic ashes (Supplementary

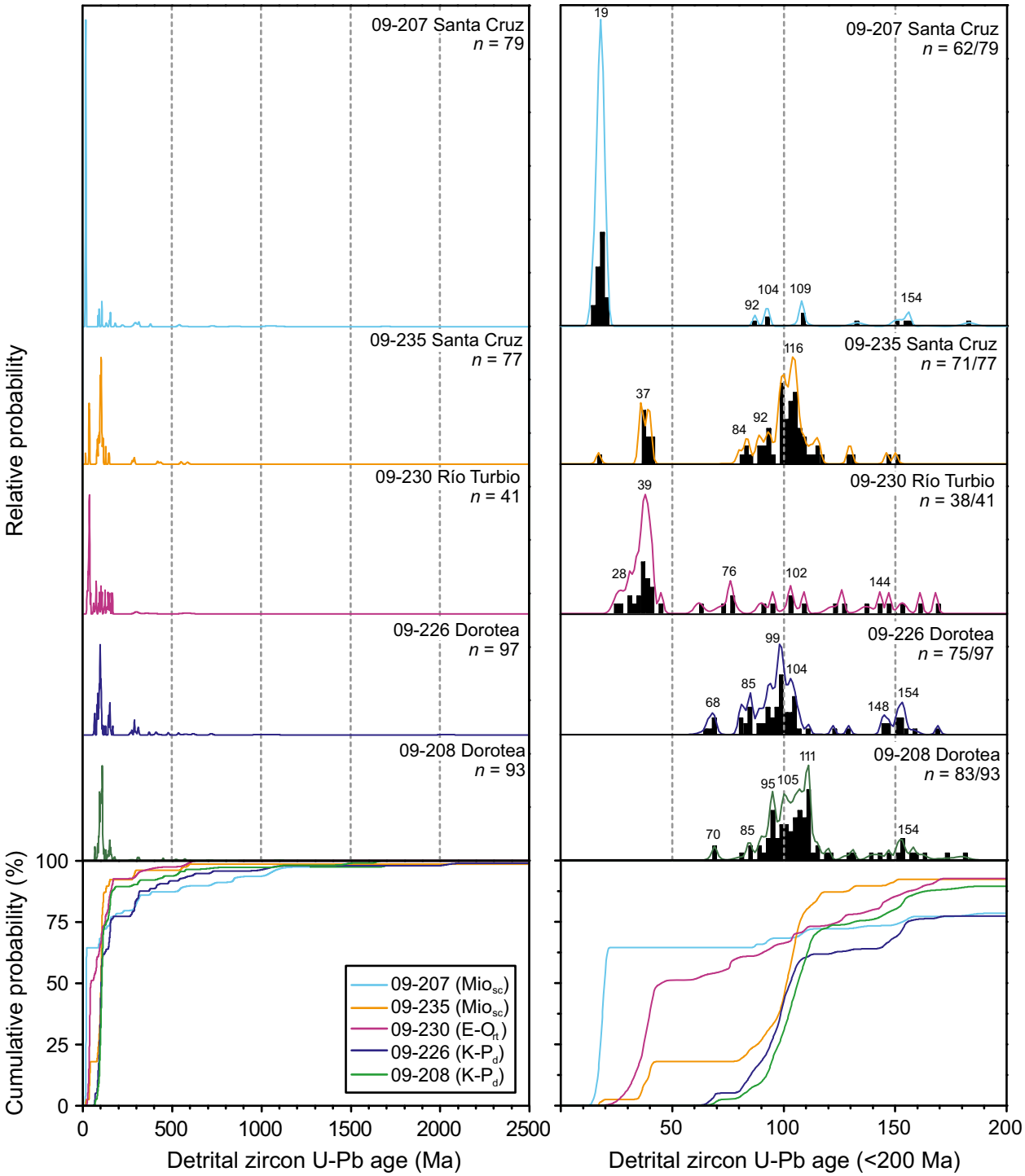

Fig. 6. Detrital zircon U–Pb crystallization ages from the Maastrichtian–Middle Miocene Magallanes foreland basinfill. Top: normalized probability distribution for all grains (left panel) and Jurassic and younger zircon (right panel) showing prominent age peaks (small numbers). Bottom plots show cumulative probability distribution for all measured zircon ages and those less than 200 Ma. K-P_d- Dorotea Formation, E-O_{rt}- Río Turbio Formation, Mio_{sc} - Santa Cruz Formation, n - number of grains <200 Ma/total grains analysed per sample.

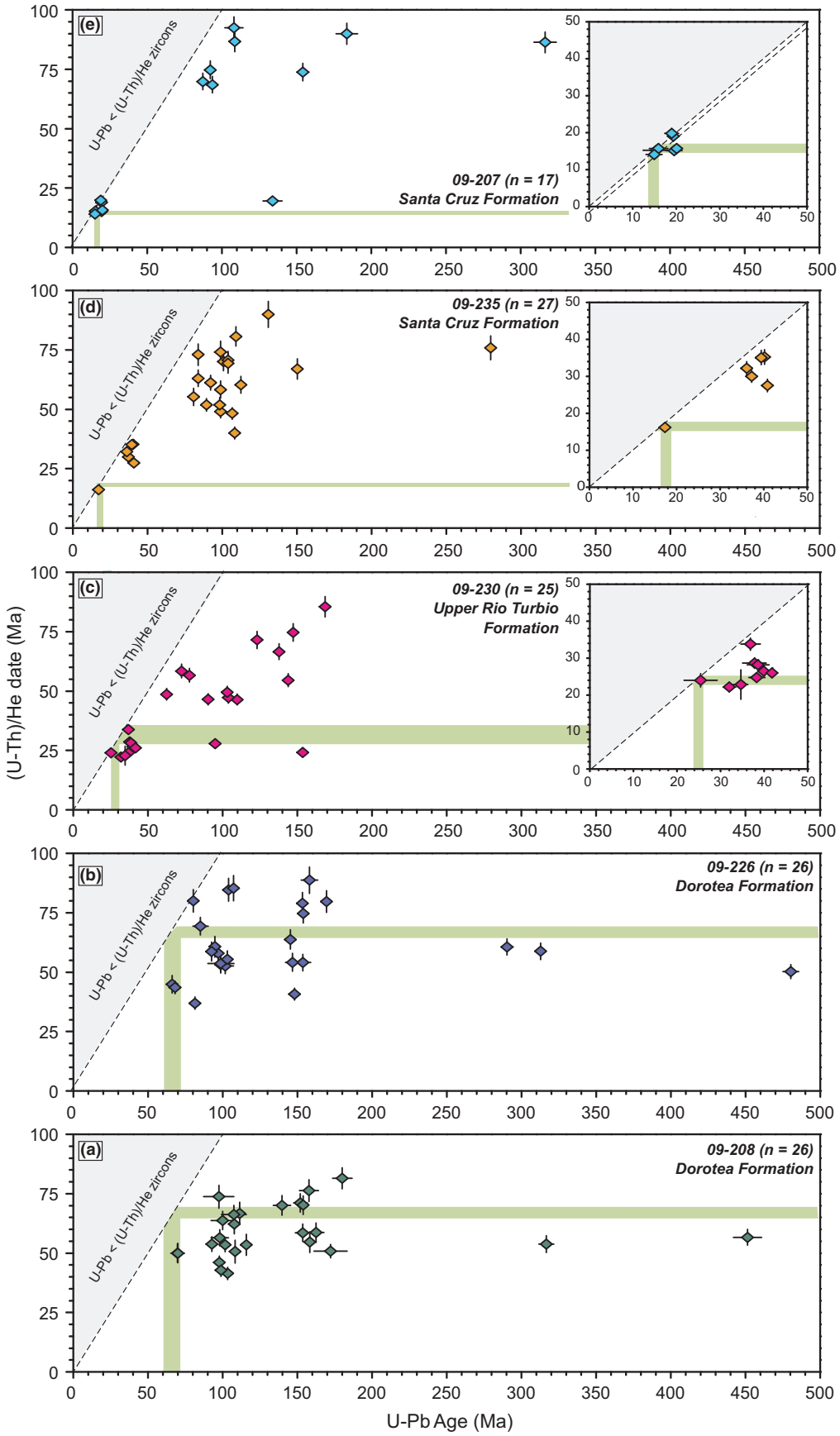

Fig. 7. Combined zircon U–Pb and He results from selected zircons from the Maastrichtian–Miocene Patagonian Magallanes foreland basinfill. Green bars indicate timing constraints on depositional age (from both palaeontology and radiometric sources). Dashed black line indicates concordant line where U–Pb and He dates are equal.

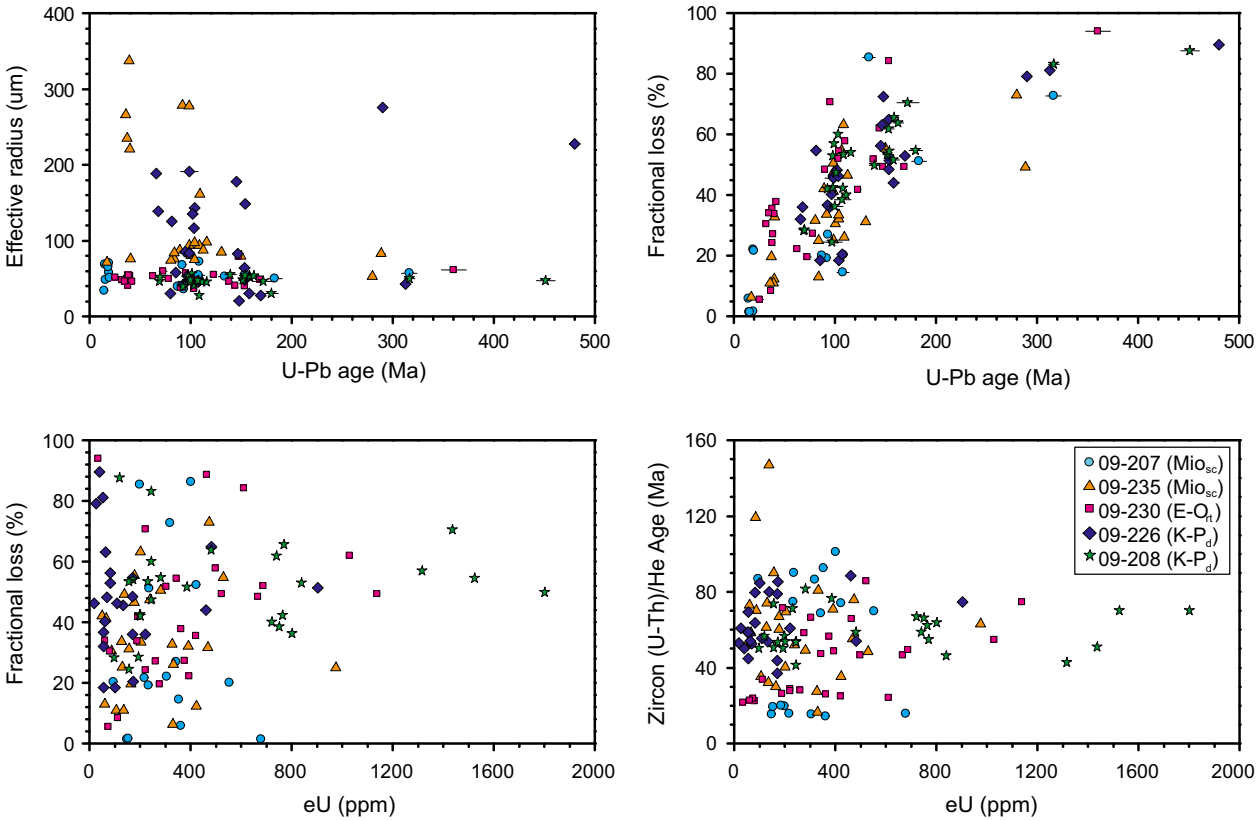

Fig. 8. Detrital zircon U–Pb and He results from the Patagonian Magallanes basin showing relationships between crystallization age (Ma), effective radius (um), fractional helium loss (%), He dates, and effective uranium concentration (eU). Most zircons have restricted effective radii between 40 and 120 μm, with scattered ages across a range of grain sizes. Data show a positive correlation between U–Pb age and fractional He loss, where youngest grains have lower levels of He loss compared to older zircon. Zircon He dates show no coherent correlation with eU.

Data). To evaluate potential influences of grain size and chemistry on thermochronology ages, we show the He dates as a function of effective grain radius (diffusive length scale) and eU in Fig. 8.

Dorotea Formation

Sample 09-208 (Río Baguales section)

Detrital zircon U–Pb ages from sample 09-208 range from 70 to 1644 Ma and are characterized by well-defined Middle Cretaceous age peaks at 70, 85, 95, 105 and 111 Ma, and a pronounced late Jurassic peak at 154 Ma (Fig. 6). Overall, about 70% of measured U–Pb ages fall between 80 and 120 Ma, with most dates clustered between 90 and 110 Ma (Fig. 6). Late Jurassic through Early Cretaceous (145–100 Ma) grains constitute an additional *ca.* 10% of the distribution, with *ca.* 20% Palaeozoic and older zircons including 275–316 Ma, 451–713 Ma and 1.10–1.60 Ga.

Twenty-seven zircons selected from sample 09-208 yielded He dates between 35 and 82 Ma (Fig. 7a). The youngest He dates (35–41 Ma) were collected from Late Cretaceous grains, whereas Middle Cretaceous grains yield a spread of He dates between 41 and 74 Ma. Late Jurassic zircons yielded slightly older He dates between 50 and 81 Ma. Two Palaeozoic zircons yield He dates between *ca.* 54 and 57 Ma, similar to the Palaeozoic zircons in sample 09-226 (Fig. 7a). All measured grains in this suite are characterized by effective radii between 28 and 56 μm and have eU values from 100 to 1803 ppm (Fig. 8). Neither parameter correlates strongly with He date (Fig. 8).

Sample 09-226 (Cordillera Chica section)

Zircon U–Pb results from 09-226 yield an age distribution from 66 to 2689 Ma that features broad Middle to Late Cretaceous age peaks (68, 85, 99 and 104 Ma), and smaller late Jurassic peaks (148 and 154 Ma) (Fig. 6). The youngest peak at 68 Ma is composed of five grains that yield concordant ages between 66 and 69 Ma, with a weighted mean of 68.6 ± 1.4 Ma. Palaeozoic grains represent 15% of the sample. These include a pronounced peak at 270–315 Ma and a broader distribution of grains between 370 and 540 Ma. Precambrian grains constitute *ca.* 6% of the distribution and exhibit 570–720 Ma, 1.0–1.06 Ga and 2.0–2.7 Ga populations (Fig. 6).

Nineteen zircons selected from sample 09-226 yielded He dates between 89–37 Ma (Fig. 7b). The youngest He dates were yielded by Late Cretaceous and one Late

Jurassic zircon. The remaining Cretaceous and Jurassic zircons yielded He dates broadly dispersed between 89 and 37 Ma. The three Palaeozoic grains yield He dates between 63 and 52 Ma. Effective grain radii for all zircons ranged from 20 to 275 μm and exhibited no correlation with He date. The eU values varied from 46 to 3464 ppm with most grains between 100 and 1000 ppm. The three grains with anomalously high eU (>1200 ppm) had Late Jurassic U–Pb ages that yielded 86–41 Ma He dates (Fig. 8).

Río Turbio Formation

Sample 09-230 (Cordillera Chica section)

Zircon U–Pb results from sample 09-230 yield ages between 25 and 584 Ma, with a minimum age peak at 28 Ma defined by four grains, a dominant Palaeogene peak (39 Ma), and with less pronounced Cretaceous peaks at 76, 102 and 144 Ma (Fig. 6). Over 50% of the analysed zircons are 25–45 Ma (Fig. 6). A few (8%) Palaeozoic and Precambrian (2%) grains are present (Fig. 6). Of the 25 selected grains from 09-230, 80% yielded He ages between 86 and 22 Ma (Fig. 7c). All Palaeogene zircons yield He dates between 22 and 35 Ma with the majority between 22 and 28 Ma. He dates from the Jurassic grains are 24–80 Ma, whereas Cretaceous grains exhibit a younger cluster of He dates between 45 and 60 Ma with one younger age (27 Ma). Effective grain radii are between 37 and 80 μm. The single Palaeozoic grain selected (not shown on Fig. 7) yields a 22 Ma (U–Th)/He date.

Santa Cruz Formation

Sample 09-235 (Cordillera Chica section)

Zircon U–Pb analyses from 09-235 range from 17 to 2622 Ma and are defined by six distinct peaks in the age distribution (Fig. 6). The youngest single grain yields a 17.3 ± 0.2 Ma (1σ) age. A prominent Palaeogene peak (37 Ma) is defined by 15% of the measured ages (Fig. 6). Most of the zircon U–Pb ages within this sample (68%) are mid-Cretaceous, with age peaks at 84, 92, 104 and 116 Ma. Late Jurassic to Early Cretaceous grains (140–150 Ma) constitute only 3% of the sample (Fig. 6). A single Palaeozoic peak at 290 Ma accounts for *ca.* 5% of the age distribution. Precambrian grains account for the remaining 5% of the sample results, in which most grains are between 550 and 590 Ma, with a single analysed 2.6 Ga grain present as well (Fig. 6).

He dates measured for the U–Pb analysed grains selected from 09-235 fall between 16 and 147 Ma (Fig. 7d). The single Miocene zircon yields the youngest He date, whereas the Palaeogene zircons yielded a narrow range of He dates between 27 and 35 Ma. Mid-Cretaceous zircons gave dispersed He dates between 40 and 120 Ma with most between 48 and 75 Ma. The several Late Jurassic and Early Cretaceous zircons selected yielded He dates between 67 and 90 Ma. The two Palaeozoic zircons yield He dates between 76 and 147 Ma (Fig. 7d). Sample 09-235 is characterized by the widest range in grain size of any of the samples. Effective radii of the grains selected for analysis range from 52 to 493 μm. Conversely, the range of measured eU for grains in this sample is relatively narrow compared to the other samples (orange triangles in Fig. 8). There is a slight correlation with grains with low eU also yielding young He dates.

Sample 09-207 (Río Baguales section)

Zircon U–Pb results from sample 09-270 yield ages between 15 and 2669 Ma, with over 60% of the analyses defining a central peak at 19 Ma (Fig. 6). The relatively minor amounts of Mesozoic and Palaeozoic zircons in this sample yield U–Pb ages similar to those described above for older samples, with age peaks at 92, 109 and 154 Ma. The proportion of Precambrian zircons in 09-207 is higher (10%) than that detected in the other samples (Fig. 6).

We measured He dates from 17 zircons in sample 09-207. All of the results fell between 14 and 97 Ma (Fig. 7e). The Middle Miocene grains all yield He dates that are nearly concordant with their respective U–Pb ages (Fig. 7e). He dates from zircons with Cretaceous and Jurassic U–Pb ages are between 60 and 95 Ma, except for a single Early Cretaceous zircon that yields an 18.8 ± 1.2 Ma (1σ) He date. The single Palaeozoic zircon yields a Late Cretaceous He date. The grain size distribution for sample 09-207 ranges from 33 to 72 μm in radius. There are no apparent correlations between He dates and grain size or eU (Fig. 8).

INTERPRETATION OF DETRITAL THERMOCHRONOLOGY RESULTS

Sediment thermal history

The availability of combined U–Pb crystallization age (ZPb) and He (ZHe) dates from the same detrital zircons provide the means to simultaneously evaluate provenance and sediment thermal history (Reiners *et al.*, 2005). In this section, we first discuss the most straight-forward interpretations regarding the thermal evolution of Magallanes basin sediment by calculating the total fractional loss of helium (*f*) in zircon relative to U–Pb crystallization age:

$$f = 1 - \left(\frac{ZHe}{ZPb}\right) \times 100 \quad (1)$$

This parameter *f* is strictly correct only for volcanic first-cycle zircons, but nonetheless is a useful measure of the grain's composite thermal evolution that permit us to classify our combined zircon U–Pb and He results from the Patagonian Magallanes basin into two categories: (1) first-cycle volcanogenic zircon or rapidly exhumed bedrock zircon with statistically similar or moderately similar

U–Pb and He ages, and (2) zircons with significant helium loss indicating protracted or complex cooling histories.

Only a small percentage of our results fall into category 1. Rapidly cooled zircons, such as those entrained in magmas erupted from volcanoes or emplaced as dikes or plutons at hypabyssal depths (<*ca.* 5 km) are both expected to yield nearly concordant U–Pb and He dates (Reiners *et al.*, 2005; Saylor *et al.*, 2012). Isotopic closure of rapidly cooled plutonic zircons can also yield nearly concordant results. Although it may be equivocal to distinguish between volcanic and rapidly exhumed plutonic zircon, such a distinction is not important to the principal goals of our study. More importantly, the clear majority of our results fall into category 2. Zircons that exhibit large fractional loss values require a more involved thermal history that could signal protracted mid-crustal residence, thermal resetting and/or tectonic burial in a basin setting (Fig. 1) (Ehlers, 2005; Reiners *et al.*, 2005).

Category 1A: First-cycle volcanogenic sources

In the Magallanes basin, the youngest detrital zircon populations typically exhibit <10% fractional loss (Fig. 8). Many of these grains have concordant U–Pb crystallization and He dates (Fig. 7). For example, both samples from the Middle Miocene Santa Cruz Formation yield abundant zircons with He dates that overlap within 2σ uncertainty of their corresponding U–Pb crystallization ages. Moreover, these zircon ages overlap with the depositional age of the Santa Cruz Formation (Fosdick *et al.*, 2011a) (Fig. 7). Following the same reasoning of Reiners *et al.* (2005) and Saylor *et al.* (2012), we conclude that these grains are likely volcanic in origin. Our assessment is supported by the presence of felsic to mafic volcanic clasts within the Santa Cruz Formation and interbedded volcanic ashes. We therefore interpret zircons with statistically concordant U–Pb and He dates that overlap the depositional age of the sediment to reflect erosion and reworking of coeval volcanic rocks and/or an ash-fall component. Similarly, we interpret the less common older detrital grains with overlapping U–Pb and He dates as rapidly cooled volcanogenic sediment.

Category 1B: Rapidly exhumed bedrock sources

Our detrital thermochronology results reveal another group of zircons that yield low to moderate *f* values (11–38%) and He dates that are within *ca.* 5–10 Myr of crystallization age (Fig. 8). Such grains are present in the Eocene–Miocene samples. For example, the Río Turbio Formation contains Eocene–Oligocene zircons that yield He dates between 35 and 25 Ma (Fig. 7c). These results are readily explained by rapid cooling to below *ca.* 150 °C soon after pluton emplacement, with continued rapid exhumation and subsequent deposition in the Oligocene basin. Similarly, this unique population is present in the overlying Santa Cruz Formation, where Eocene–Oligocene grains yield comparable low levels of fractional loss and He dates between 35 and 25 Ma (Fig. 7c). We propose that the Eocene–Oligocene zircons were derived from the magmatic arc, where high exhumation rates facilitated erosion and transport of these sediments eastward and northward into the foreland basin. The Oligocene zircon populations in sample 09-230 require further investigation into a revised depositional age of the Río Turbio Formation, and/or a minor component of post-depositional helium loss.

Category 2: Sediment with protracted thermal histories

The majority of the analysed Mesozoic and Palaeozoic grains in the Magallanes basin – in the whole Cenozoic sample suite – exhibit moderate to high fraction loss values (24–97%) and large age differences between U–Pb and He dates (85–40 Ma) (Fig. 7). Several important observations can be made. First, radiation damage alone cannot account for the observed patterns. Second, many of the He dates from the older strata are younger than the depositional age of the sediments themselves.

The first observation is important because some studies have identified circumstances in which radiation damage during alpha-decay produces complex relationships between He date and effective uranium concentration eU (e.g. Shuster *et al.*, 2006; Flowers *et al.*, 2009; Guenthner *et al.*, 2013). The possibility of such behaviour tends to naturally increase with U–Pb crystallization age because greater time allows more radiation damage to occur. Given the comparatively young grains and relatively low eU materials that we have analysed (Fig. 8), the lack of strong correlation between He date and eU for our samples allows us to rule out radiation damage as a dominant factor for the vast majority of our results, although it may account for some of the scatter within modelled He dates.

A substantial number of zircon He dates (30% of grains) from the Maastrichtian Dorotea Formation (including representatives of all important U–Pb age populations) yield He dates that are younger than depositional age. This relationship, observed in both Dorotea samples (Fig. 7), indicates a major control for post-depositional burial heating of the Maastrichtian basinfill upon He loss in zircons. This observation strongly implies that the Dorotea Formation samples share a basin thermal history that was substantially above *ca.* 150 °C (e.g. Reiners *et al.*, 2005). If basin burial temperatures exceed the upper bound of the zircon He PRZ (*ca.* 200 °C), grains are fully outgassed and all prior He thermal history below this temperature is erased. This produces uniform He dates that reflect the final stages of basin heating and cooling through He closure. The significant spread of individual He dates recorded by our samples precludes burial temperatures from having exceeded *ca.* 200 °C. In addition, the lack of He dates younger than 40 Ma for pre-Cenozoic zircons requires that the major heating event in the Palaeocene Magallanes basin occurred between deposition at *ca.* 60 and 40 Ma.

Conceptual approach for thermal modelling

The premise for our numerical thermal model is that sediments that undergo basin heating will share a common phase of thermal history, superimposed on the individual, prebasin detrital cooling histories derived from source areas. Given the substantial degree of post-depositional partial resetting of He dates in the Dorotea Formation, we focus our modelling on quantifying the timing and magnitude of the shared basin phase. When diffusive He loss during basin heating is comparatively minor and temporally well-constrained, it is possible to extract the original sediment source thermal history information from individual grains by applying a common correction for basin heating (e.g. Reiners *et al.*, 2005). Similarly, simple interpretations are also possible when post-depositional heating is sufficient to completely outgas zircon, leading to reset He dates. However, a fundamental problem that limits meaningful forward modelling of basin heating for combined U–Pb and He detrital zircon data sets is a lack of constraint upon the prebasin thermal history for individual grains. This problem is made smaller to the extent that basin heating is the predominant control upon He loss in zircon. Nevertheless, efforts to constrain the magnitude and timing of basin heating will need to simulate the prebasin thermal history to correct for it.

There are a variety of approaches for numerically modelling thermochronology data (e.g. Ketcham, 2005) that take into account both diffusive loss and radiogenic ingrowth for a particular grain. As numerous nonunique temperature–time solutions exist for a single fractional helium loss value, our approach leverages the combined U–Pb and He data set to assess the magnitude of reheating using all grains. To quantify the magnitude of basin burial heating and assess the range of plausible thermal histories for these sediments, we developed a simple numerical model that incorporates He ingrowth and diffusion in terms of basin reheating and prebasin (sediment source) cooling (Fig. 9). The range of possible temperature–time histories is restricted through the use of available geologic constraints on the depositional age and setting, sedimentary provenance, and tectonic deformational history for the Patagonian Andes.

Model design and parameters

This modelling approach exploits the relationships between the Arrhenius behaviour for thermally activated volume diffusion and the Fourier number (F_0) obtained from fractional loss equations (Mcdougall & Harrison, 1999 and references therein). The fractional loss (f) of a grain during episodic helium loss at

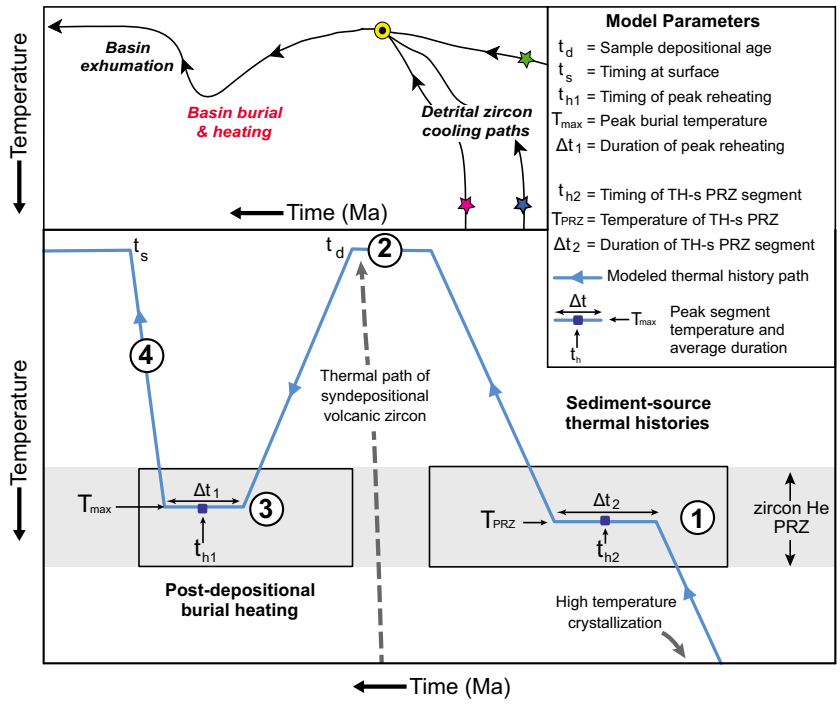

Fig. 9. Model setup for forward modelling of thermal histories using detrital thermochronologic data. Top panel shows conceptual thermal evolution from Fig. 1. Two heating stages are modelled: the prebasin thermal history of sediment source represents thermal conditioning of zircon during post-emplacement cooling and exhumation prior to deposition in the foreland basin. The second heating phase represents post-depositional burial heating and subsequent basin exhumation. Geologic constraints provide fixed model parameters that include sample depositional age (t_d), erosional unconformities and/or age of overlying strata (t_s) and the temperature bounds defined by the zircon He PRZ. For numerical simplicity, the youngest and oldest ZPb ages define the temporal boundary on the Source thermal history thermal window. Forward modelled thermal paths are defined by the timing (t_h) and duration (Δt) of the peak basin heating (T_{max}) using incremented 2 °C temperature steps and 2 Myr time steps.

constant temperature is a function of the dimensionless Fourier number (F_o) characterizing the volume diffusion (eqn 2),

$$F_0 = \frac{Dt}{r^2} \tag{2}$$

where $D = D_o\, e(-E/RT)$ is the thermally activated diffusion coefficient, E is the activation energy, R is the gas constant, D_o is the frequency factor, T is the temperature, r is the effective diffusive length scale for He in the grain and t is the duration of the square pulse heating (Mcdougall & Harrison, 1999). For spherical grain geometry, the total fractional loss of He is characterized by:

$$f = C_0 - 6/\pi^2 \sum_{n=1}^{\infty} (1/n^2)[1 - I_n] \tag{3}$$

where C_o is the total normalized He produced since crystallization and I_n is the convolution integral of the production and diffusion factors (see Lovera *et al.*, 1989; Mcdougall & Harrison, 1999):

$$I_n = e^{-\alpha_n^2 F_0} + \alpha_n^2 \int_0^{F_0} e^{-\alpha_n^2 (F_0 - x)}\, dx \tag{4}$$

where $\alpha_n = n\pi$ and λ is an effective He decay constant. To model geologically meaningful thermal histories such as those in a foreland basin, the Fourier coefficient is replaced by the time integration of the diffusion coefficient $D(T)$:

$$F_0 = \int_0^t \frac{D(T(t'))}{r^2}\, dt' \tag{5}$$

Given a thermal history since the time of crystallization (t_o = measured zircon U–Pb age), F_o is completely determined from eqn (5), and the He fractional loss can be calculated using eqns (3) and (4). The apparent He date of the sample is then calculated from equation:

$$\text{Age} = \lambda^{-1} \ln(1 + (e^{\lambda t_0} - 1)(1 - f)) \tag{6}$$

For detrital grains, we make the simplifying assumption that they share the same diffusion properties and compare them with the measured (alpha ejection-corrected) He dates. For grains buried in a foreland sedimentary basin and subsequently exhumed during thrust advancement, we prescribed a simplified eight segment T-t path for our model that characterizes sediment source cooling, basin reheating to a peak temperature (T_{max}) and basin exhumation (Fig. 9). In *stage 1*, zircon grains crystallize in the magmatic arc and cool through intermediate temperatures during unroofing to the Earth's surface (Fig. 9). During *stage 2*, sediment is eroded and transported to the foredeep depozones of the Magallanes foreland basin (Fig. 9). *Stages 1* and *2* together constitute the older 'source thermal history' in our model. Once in the basin, the sedimentary layer and detrital grains undergo a shared basin thermal history that includes basin burial heating and residence at maximum burial temperature in *stage 3*, and subsequent basin exhumation to the surface in *stage 4* (Fig. 9).

The following steps summarize the modelling workflow for iterative calculation of model thermal histories and associated He dates:

Step 1: Define the searchable T-t space for the thermal history paths using sample depositional age (t_d), erosional unconformities and/or age of overlying strata (t_s) and the temperature bounds defined by the zircon He PRZ. For numerical simplicity, the youngest and oldest ZPb ages define the temporal boundary on the source thermal history window. Forward modelled thermal paths are defined by the timing (t_h) and duration (Δt) of the peak basin heating (T_{max}) using incremented 2 °C temperature steps and 2 Myr time steps (Fig. 9).

Step 2: For each modelled thermal path, calculate an apparent He date for each grain, using the accumulation and diffusion of helium since the time of crystallization age.

Step 3: Compare the modelled distribution of apparent He dates to the measured distribution of He dates using the Kolmogorov–Smirnoff (K–S) statistical test (Press *et al.*, 1989) for populations.

Step 4: Repeat Steps 2 and 3 for each defined thermal path (n = 70 000).

Step 5: Select best-fit model results using K–S probability test with probabilities greater than 0.68. For visualization purposes, plot the average age (t_h) and duration (Δt) for peak basin temperatures (stage 3) and prebasin PRZ segments (stage 1) for best-fitting results.

The numerical model is calibrated using measured grain dimensions to approximate the effective diffusion radius r (Table S3), activation energy E = 40.4 kcal mol^{-1} and diffusivity D_0 = 46 mm^2 sec^{-1} for He diffusion parameters in zircon (Reiners *et al.*, 2004). Running the model for the range of prescribed thermal histories (e.g. *ca.* 70 000) identifies a subset of paths that satisfy the measured fractional loss values and measured ZHe age of each grain in a detrital sample. We compare the model results with measured He data by employing K–S statistic on the calculated cumulative zircon He date distributions as a goodness-of-fit criterion (e.g. Lovera *et al.*, 1999; Cina *et al.*, 2009). Input parameters and model results for each sample are reported in the Supporting Information.

Thermal modelling results

Hypothetical burial heating. To illustrate the effects of basin heating on a suite of Mesozoic detrital zircons, we first calculate He dates for a 10 Myr square pulse heating event between 50 and 40 Ma (Fig. 10). Zircon U–Pb ages and measured grain sizes are based on sample 09-208. Results show progressive younging of He dates with

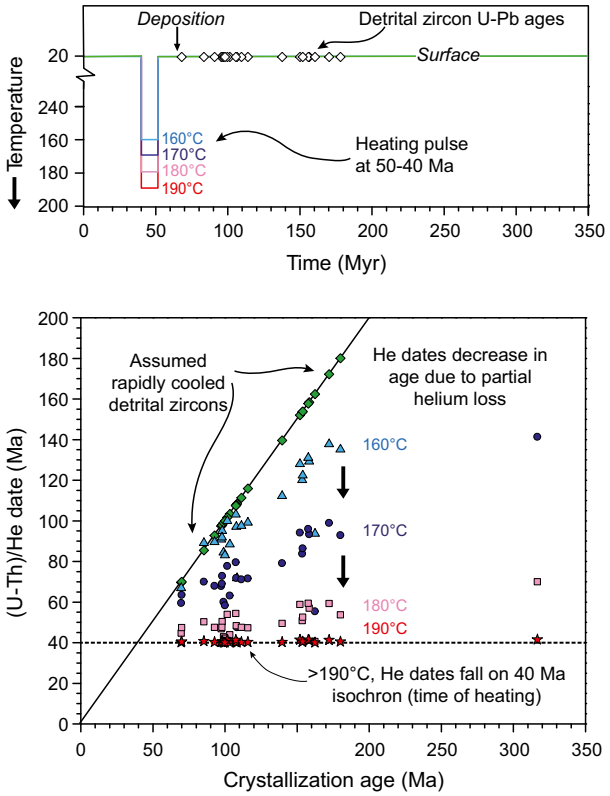

Fig. 10. The effect of progressive burial heating on a Maastrichtian detrital zircon sample. In this simple example, initial zircon He dates are assumed to be equal to U–Pb ages as a result of rapid post-emplacement cooling (green diamonds). Top panel shows a schematic square pulse heating event between 50 and 40 Ma. White triangles show U–Pb age distribution of detrital zircons. As peak temperature of the heating pulse increases, He ages decrease and the detrital sample exhibits scatter in helium dates (blue triangles, purple circles and pink squares) related to diffusion properties such as individual grain size and chemistry. At high temperatures >190 °C, all He dates have been sufficiently reset and fall on the 40 Ma isochron (red stars) and record the end of the heating episode. Modelled data are based on detrital U–Pb ages and grain sizes (effective radii) from sample 09-208.

increasing temperature. In this simple example, we assume that initial detrital zircons were rapidly cooled and had restricted helium loss (<10% for green diamonds on 1:1 line) prior to deposition (Fig. 10). As basin heating progresses, the suite of He dates decreases and develops a spread in age that reflects intrinsic diffusive heterogeneity of individual zircons (such as diffusive length scale). At higher temperatures within the PRZ *ca.* 190 °C, zircon is nearly fully degassed of radiogenic He and record a uniform cluster of He dates at 40 Ma that reflects the end of the heating pulse (red stars) (Fig. 10). Although these calculations are performed for a single heating event with a single square pulse thermal history, they effectively demonstrate how detrital zircon He dates respond to progressive basin heating at different isothermal conditions.

Basin heating of Maastrichtian Magallanes strata. Numerical modelling results for zircons from the Maastrichtian Dorotea Formation yield best-fit temperature–time paths that produce model He dates with a broadly overlapping spread of measured He dates (Fig. 11). Figure 11A presents the 180 best-fit results from 74 880 model runs, each of which fit the population of zircons for a unique thermal history for a K–S statistic of probability >0.68. Model results indicate that Cenozoic post-depositional basin heating reached peak temperatures between 164 and 180 °C that were attained between 54 and 45 Ma. The mean values for all best-fit basin thermal paths indicate a post-depositional peak temperature of *ca.* 175 °C centred at *ca.* 45 Ma. In the light of the dispersive behaviour of detrital He dates for a simple square pulse burial thermal history (e.g. Fig. 10), the thermal model results for sample 09-208 are a successful first-order approximation for the total magnitude of fractional loss (Fig. 11b). Some individual grain results show more scatter between modelled and measured ages. We attribute this scatter to variable diffusive properties of the grains and heterogeneous source thermal histories of individual grains, neither of which are considered in this simple model. Nonetheless, the coherence of the measured vs. model He results confirm that the thermal history of the majority of detrital zircons from this sample was strongly influenced by basin thermal history.

Although our modelling design makes simplifying assumptions for the predepositional temperature–time segments of individual grains, results show that a broadly defined range of predepositional thermal histories are required to achieve acceptable He dates (Fig. 11a). For these older source thermal histories, results indicate that most Mesozoic grains had already cooled below 180 °C by at least Late Cretaceous time. As grains derived from syndepositional volcanism are assumed to have essentially zero fractional helium loss prior to deposition, we are able to rely heavily on the zircon population with youngest U–Pb ages (*ca.* 68 Ma) to constrain the maximum extent of basin burial heating. Best-fit thermal histories yield model He dates for these young grains that are slightly older than measured dates (Fig. 11b), suggesting that the magnitude of basin heating phase constrained by the model using all detrital grains may be a minimum.

The model ages of some grains deviate significantly from measured He dates. Although the spread of ages can be influenced by individual zircon grain characteristics such as individual grain diffusive properties or misrepresentation of diffusive length scale (grain radius) (e.g. Flowers *et al.*, 2009; Guenthner *et al.*, 2013), we note no strong correlation between these factors and therefore consider them relatively minor influences. Alternatively, we hypothesize that this misfit reflects important differences in predepositional thermal histories relative to that experienced by the majority of grains in the distribution. For instance, a group of older Jurassic grains generally have younger modelled best-fit ages than measured ages (Fig. 11b), suggesting that their individual bedrock source thermal histories were likely higher in temperature, longer in duration and/or younger than other grains.

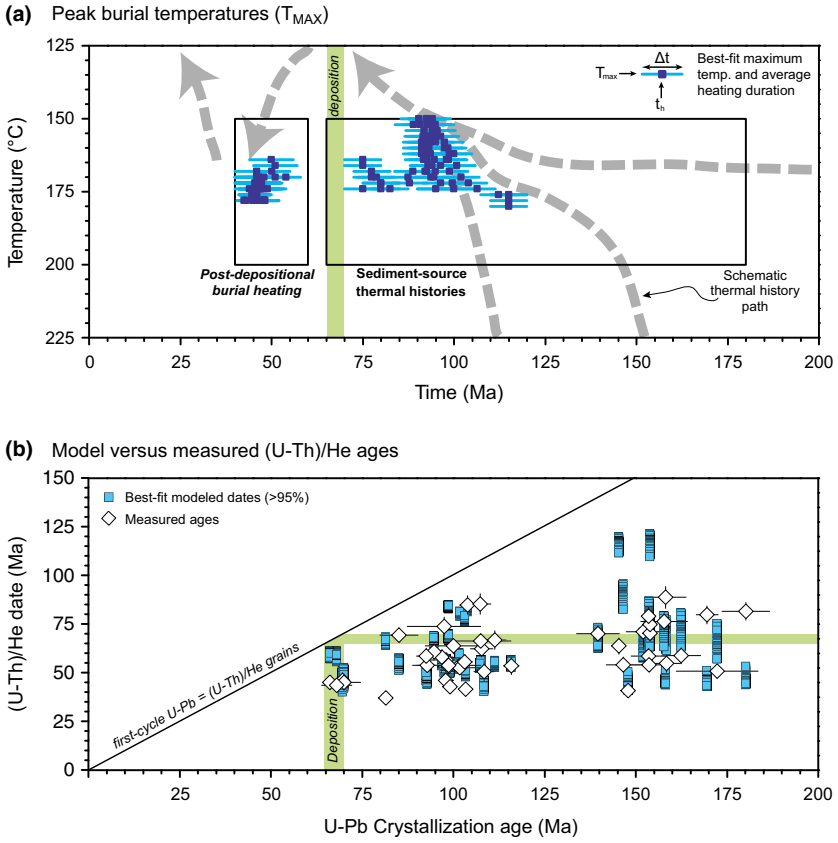

Fig. 11. Thermal modelling results for burial heating of detrital zircons from the Dorotea Formation (sample 09-208). (a) Best-fit peak temperatures (T_{max}) for all prescribed thermal histories that satisfy the K–S goodness-of-fit statistical test with probability value >0.68. Blue line segments show the average heating duration for each peak temperature. Superimposed dark blue squares show central age of each T_{max} segment. (b) Comparison of best-fit modelled zircon He ages (vertical blue bars) and measured zircon (U–Th)/He dates (grey diamonds).

Although these estimates are based on best-fit thermal model results within the geologic context of the basin succession, one significant source of complexity arises from the uncertainty of the depositional age of overlying Middle Eocene–Oligocene(?) Río Turbio Formation. Specifically, its lower age bracket from correlative units elsewhere in the Andes (Otero *et al.*, 2012) coincides with the age range of reported zircon He dates and timing of burial heating. Additional chronostratigraphy of the Palaeogene strata would improve our estimates of burial heating and elucidate the significance of unconformities developed within the basin succession.

Thermal histories of Middle Miocene sediment sources. The observation that all measured Jurassic–Cretaceous grains from the Cenozoic sediments define a relatively restricted range of zircon He dates between *ca.* 80 and 40 Ma provide a strong indication that sediment sources had a broadly similar thermal history to the Maastrichtian Dorotea Formation. We consider the thermotectonic history of the Cretaceous strata exposed in the thrust belt and hypothesize that these rocks were a predominant source of recycled sediment to the Cenozoic basin. To test this hypothesis and constrain the plausible thermal histories of Miocene sediments, we performed thermal modelling on the Mesozoic zircons from the Middle Miocene Santa Cruz Formation (Fig. 12).

Results for 78 880 model runs of Mesozoic zircons from combined samples 09-207 to 09-235 are shown in Fig. 12 and portray the permissible temperature–time histories capable of reproducing the observed He data distributions for Cretaceous and Jurassic zircons. Best-fit results (n = 215 model runs for K–S probability >0.68) suggest peak temperatures during Palaeocene heating of *ca.* 160–180 °C that were reached between 55 and 44 Ma, and a broad temporal range of Cretaceous thermal histories (Fig. 12a). Respective modelled He dates for these thermal histories yield overall compatible range of dates, although single grain discrepancies are evident. Specifically, the best-fit results for late Cretaceous and Jurassic grains overestimate the degree of fractional loss and yield model He dates *ca.* 10% younger than measured dates (Fig. 12b). Mid-Cretaceous grains, in contrast, are slightly older than model results, suggesting differences in sediment source thermal histories that are not resolved by the model (Fig. 12b).

Figure 13 compares the best-fit thermal histories for the Palaeogene basin heating from both the Maastrichtian Dorotea Formation (blue) and thermal histories calculated for grains inferred to have been recycled from older Magallanes basin fill into Middle Miocene (orange) depositional systems. Given the considerable similarity between modelled thermal conditions for these samples and previous consistent He results from deeply exhumed Magallanes basin strata (Fosdick *et al.*, 2013), we conclude that it is highly likely that the Patagonian Miocene depocentre received significant recycled detritus derived from deeply buried, Cretaceous basinal strata that were uplifted and eroded as the thrust belt evolved.

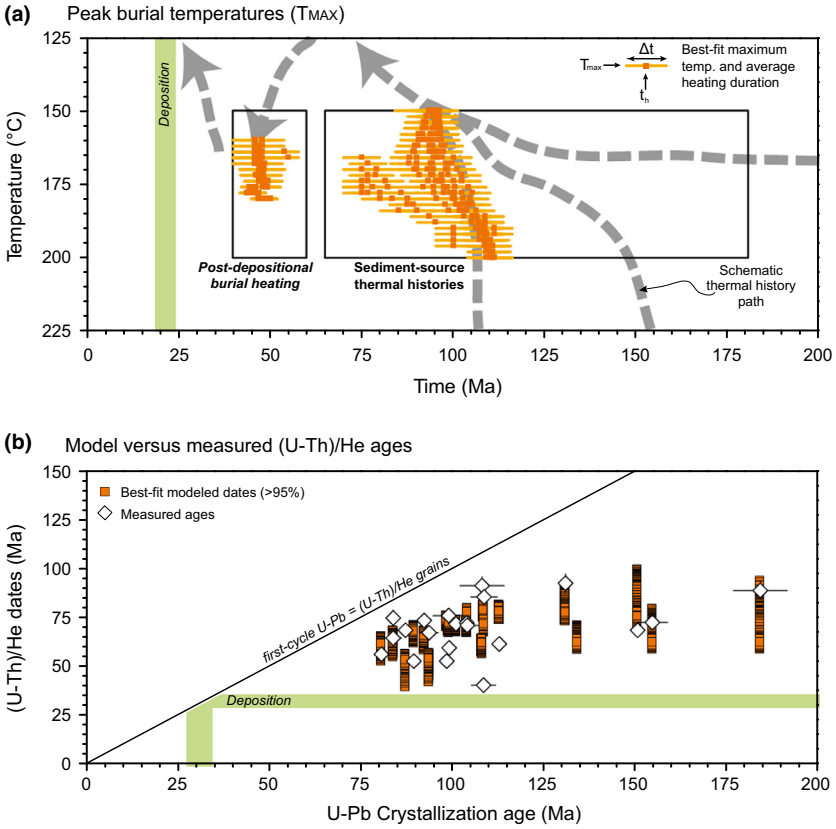

Fig. 12. Thermal modelling results for the Middle Miocene basinfill for thermal conditions that reflect burial and exhumation in the Cretaceous foredeep. Only the Mesozoic zircons are modelled to test sediment recycling. (a) Best-fit peak temperatures (T_{max}) for all prescribed thermal histories that satisfy the K–S goodness-of-fit statistical test with probability value >0.68. Orange line segments show the average heating duration for each peak temperature. Superimposed dark blue squares show central age of each T_{max} segment. (b) Comparison of best-fit modelled zircon He ages (vertical orange bars) and measured zircon (U–Th)/He dates (orange diamonds).

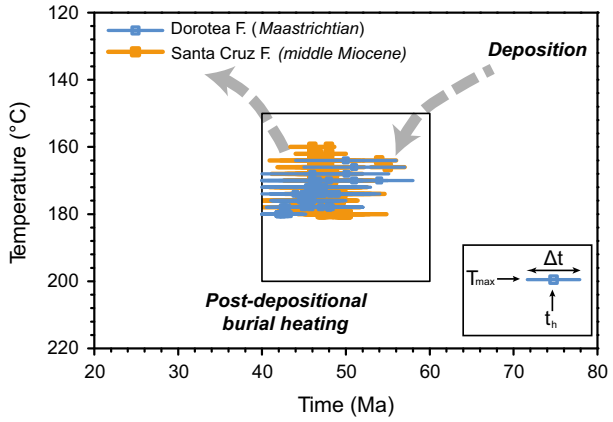

Fig. 13. Comparison of thermal modelling results for the buried Cretaceous Dorotea Formation (blue) and recycled sediments (Mesozoic zircons only) in the Middle Miocene Santa Cruz Formation (orange). Refer to Figs 11 and 12 for individual sample modelling results. Similar best-fit thermal histories for the Palaeogene basin heating stage are consistent with our interpretation that the Neogene basin received sediment derived from orogenic recycling of the deeply buried Cretaceous strata exposed in the thrust belt.

DISCUSSION

Geodynamic implications of Palaeocene–Eocene thermotectonic evolution

The retroarc foreland basin of an orogenic belt is a dynamic region in which sediments can be deposited, buried and underthrust, and subsequently exhumed as the orogen evolves (Fig. 14). The Palaeogene thermotectonic record in the Patagonian Magallanes basin is one of the least understood stages, due in part to an incomplete stratigraphic record and lack of clearly dated Palaeogene structures in the thrust belt. Our detrital geochronology and thermochronology findings illuminate major changes in sediment source areas from the Cretaceous history into early Cenozoic events and constrain an important Palaeogene thermal history resolved in the partially reset He dates and thermal modelling. By integrating our provenance and thermochronology findings with structural reconstructions and palaeoenvironmental data, we are able to develop a simplified palaeogeographic reconstruction of major Maastrichtian–Neogene tectonic events that affected the studied areas of the Patagonian batholith, thrust belt and foreland basin (Fig. 14).

The foredeep sediment dispersal system in the Patagonian Magallanes basin was stable throughout Maastrichtian time, during southward progradation of the shelf-slope system and deposition of the Dorotea Formation (Fig. 14a) (Covault *et al.*, 2009; Romans *et al.*, 2009; Hubbard *et al.*, 2010; Romans *et al.*, 2010). For the shoreface sandstone lithofacies, the similarity in zircon provenance signature throughout the entire *ca.* 1000 m thick formation indicates no major shift in source region during *ca.* 10 Myr interval of southward basin-filling (Fig. 14a). The mid-Cretaceous batholith persisted as an important sediment source during this time. In addition, the remarkable similarity between detrital zircon

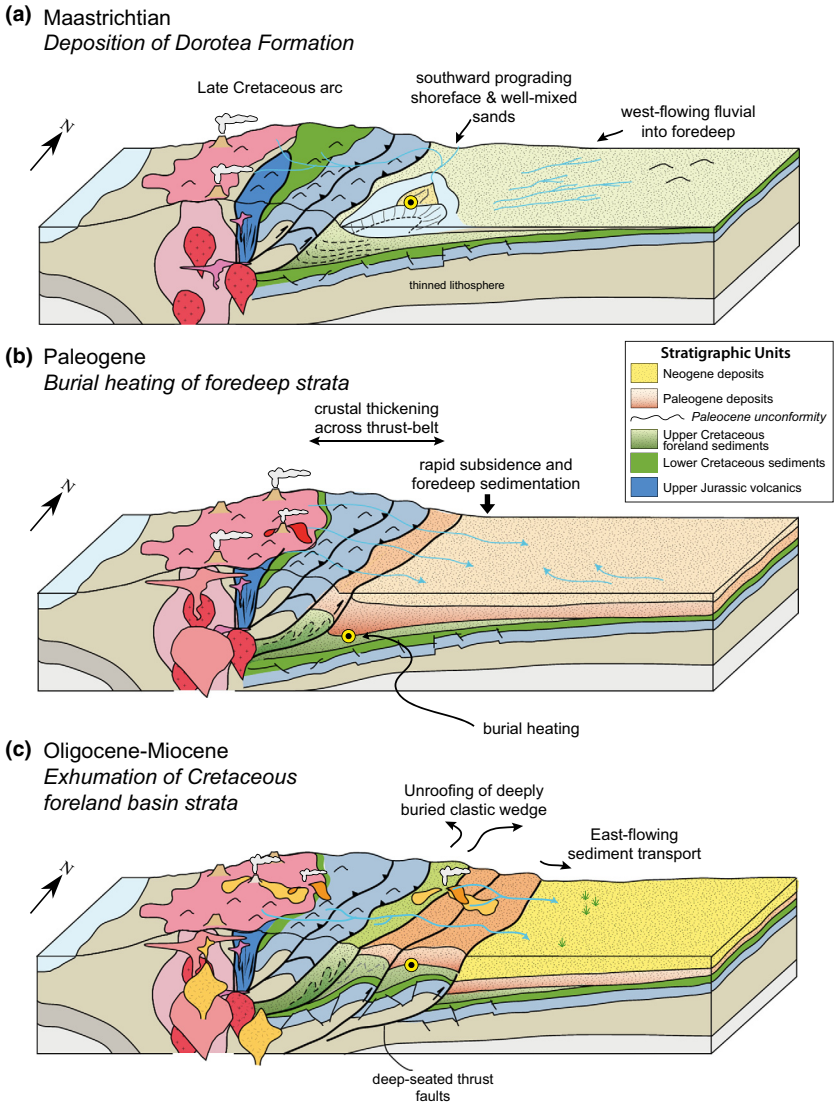

Fig. 14. Schematic depiction of palaeogeographic evolution of the Patagonian thrust belt and Magallanes basin showing tectonic structures, sediment dispersal systems and lithotectonic terranes during (a) Maastrichtian deposition of Dorotea Formation, (b) Palaeogene burial of foreland basin deposits during rapid sedimentation and tectonic loading and (c) Oligocene–Miocene propagation of thrust front and unroofing of the Cretaceous clastic wedge. Refer to Fig. 2 for approximate location of section.

distributions within the upper Dorotea Formation for at least *ca.* 80 km along depositional dip (between the Río Baguales and Cordillera Chica study areas) suggests that the Palaeocene shelfal sands were thoroughly mixed during southward progradation of the shelf.

Our temperature–time modelling of combined U–Pb and He results indicate that the Dorotea Formation achieved post-depositional burial temperatures between *ca.* 164 and 180 °C, and between 54 and 45 Ma (Fig. 11). Although other thermal indicators from these outcrops are currently lacking, this magnitude of burial heating for the Maastrichtian deposits is surprisingly high, given the restricted thickness of stratigraphic overburden along the Andean foothills (Fig. 5). Sparse vitrinite reflectance values of *ca.* 0.5%Ro obtained from outcrops of the Upper Cretaceous Tres Pasos Formation, exposed near Cerro Castillo (Fig. 4), have been modelled to infer only *ca.* 2 km of stratigraphic overburden at this location (Skarmeta & Castelli, 1997 and references therein). More recently, zircon He data from these rocks indicate that these strata have been subjected to post-depositional temperatures within the zircon He PRZ (*ca.* 140–190 °C), and stratigraphically deeper rocks exposed in the thrust belt yield zircon He dates that yield entirely thermally reset Early Miocene dates (Fosdick *et al.*, 2013).

We consider three plausible geologic explanations for regional burial heating of the Dorotea Formation: (1) tectonic burial by advancing thrust sheets, (2) regional heating by mafic plateau volcanism and (3) sedimentary burial in an actively subsiding foredeep. Structural repetition of the Upper Cretaceous stratigraphy is reported in the western domain of the Patagonian thrust belt (Wilson, 1991; Skarmeta & Castelli, 1997; Kraemer, 1998; Fosdick *et al.*, 2011a). However, evidence of major over-thrusting is not apparent across the eastern flanks of the Patagonian thrust belt, where outcrop and subsurface data depict a monoclinal belt of gently east-dipping strata (Biddle *et al.*, 1986; Harambour, 2002; Fosdick *et al.*, 2011a). Although thrust faulting within the Dorotea Formation has led to a small component of thickening within this monocline belt, over-thrusting alone is an insufficient explanation for burial heating.

Palaeogene heating observed in the Dorotea Formation could be attributed to regional mafic volcanism that has been documented in Patagonia. Eocene collision of the Farallon-Aluk-spreading centre with the Chile trench has been invoked to explain Eocene mafic lavas in Patagonia (Nullo *et al.*, 1993; Kay *et al.*, 2002; Ramos & Kay, 2002). Although Eocene volcanic rocks have yet to be identified as far south as the Río Baguales and Cordillera Chica study areas, elevation in basal heat flow due to the spreading centre may have contributed to heating of the Dorotea Formation. Local geochronology has not identified these volcanics, although undated basaltic sills in the Río Baguales merit further investigation of this mechanism. However, we note that mafic intrusive volcanics are not observed in the Cordillera Chica area, and yet along the depositional axis, the similarity in overall timing and magnitude of partial resetting and basin heating of the Maastrichtian sediments suggests that the foredeep trough underwent concurrent subsidence and burial, thereby requiring a regional mechanism for heating.

An alternative and our preferred explanation is that the deep burial responsible for the post-depositional heating was largely depositional and driven by flexural foreland subsidence and sustained high rates of sediment supply during Late Cretaceous and early Palaeogene time (Fig. 14b). In addition, high heat flow during Eocene magmatism very likely affected the thermal regime and led to elevated geothermal gradients as well. Using an average 30 °C km^{-1} geothermal gradient for Patagonia (based on measured heat flow from Hamza & Muñoz, 1996) and a surface temperature of 20 °C, the modelled 164–180 °C peak temperatures correspond to 4.8–5.3 km burial depths (see supplementary materials for full calculations).

Such a burial heating mechanism is attractive in the light of the fact that the Patagonian Magallanes basin features a regionally developed erosional unconformity above Maastrichtian deposits. The preserved post-Palaeocene sedimentary succession is insufficiently thick (*ca.* 800–2500 m) to explain the magnitude of observed basin heating, however, the *ca.* 25 Myr stratigraphic gap permits an unknown thickness of overburden to have been deposited and later removed (Biddle *et al.*, 1986; Malumián & Náñez, 1988; Malumián *et al.*, 2000). Palaeogene basin burial and heating followed by rapid erosional removal of *ca.* 5 km of overburden has important tectonic implications for thrust belt – foreland basin interactions in the foreland region.

For the end-member conditions of Early Eocene peak burial temperatures of *ca.* 164–180 °C, we estimate decompacted sediment accumulation rates of *ca.* 0.3–0.5 mm $years^{-1}$ (see Supplementary Information). These first-order estimates do not account for transient cooling due to rapid deposition of sediments, but are considered here as minimum sedimentation rates required for deposition of *ca.* 5 km overburden between 70 Ma and peak burial between 54 Ma and 46 Ma. In contrast, rapid erosion rates (*ca.* 0.5–2.7 mm $years^{-1}$) are required to remove this stratigraphic overburden prior to deposition of the Man Aike/Río Turbio Formation in Middle Eocene time. These estimated sediment accumulation and erosion rates are typical of high rates documented elsewhere in actively deforming orogenic belts and efficient sedimentary routing systems (e.g. Einsele *et al.*, 1996), and are thus permissible for the burial and unroofing interpretation of the Patagonian Magallanes basin.

Our combined zircon U–Pb and He results shed light on the nature of Palaeogene events in the Patagonian Andes during an interval where the sedimentary record preserves no direct information (Malumián *et al.*, 2000). Further south, the Palaeocene–Eocene tectonic evolution of the Tierra del Fuego region includes a period of active basement thrust faulting, internal deformation (Ghiglione and Ramos, 2005; Klepeis *et al.*, 2010), and major unroofing of the orogen to supply sediment to the Palaeocene and Early Eocene depocentre (Biddle *et al.*, 1986; Barbeau *et al.*, 2009); Zahid & Barbeau, 2010). Thermochronology performed in this region has documented an important episode of Palaeogene exhumation of the Cordillera Darwin and a similarly timed phase of hinterland thrusting (Kohn *et al.*, 1993; Gombosi *et al.*, 2009). Although the Palaeocene–Middle Eocene sedimentary record is missing at the latitude of our study area in the Magallanes basin, we regard it very plausible that despite differences in kinematic history, synchronous deformation and active sedimentation were operating in the Patagonian orogenic segment and led to enhanced foreland subsidence and sedimentation during Palaeogene time.

The development of the Magallanes basin on thinned lithosphere during Late Jurassic backarc rifting has important geodynamic implications for subsidence and sediment thickness distributions. Flexural modelling of the Cretaceous Patagonian foreland subsidence suggests that weakened crust and lateral variations in strength can explain the unusually thick foredeep deposits (Fosdick *et al.*, 2011b). Moreover, crustal heterogeneities promote episodic depocentre migration behaviour, in which prolonged periods of subsidence and sediment accumulation are terminated by abrupt depocentre migration, causing foreland uplift and widespread erosional bevelling of foredeep strata (Waschbusch & Royden, 1992; Fosdick *et al.*, 2011b). The exceptional magnitudes of burial heating and subsequent uplift and erosion that we report should be considered as possible diagnostic features of convergent basins that develop on similarly attenuated convergent settings elsewhere. The overall exhumation depths exhibited by the frontal margin of the Patagonian thrust belt are unusually large compared to other segments of the Andean orogenic belt. In the south central Andes, for example, frontal thrust sheets have been exhumed from relatively shallow crustal depths < 4-5 km and uplifted Cenozoic basinfill strata preserve detrital zircon He age distributions (Fosdick & Carrapa, 2012).

Neogene sediment recycling and eastward migration of the drainage divide

The character of the foreland basin system in Patagonia changed markedly after Late Eocene time and sedimentation shifted eastward, where predominantly shallow to nonmarine conditions persisted throughout the Neogene (Fig. 14c). Foreland thrust propagation in Oligocene and Early Miocene time resulted in a wider orogenic belt that provided sediment to east-directed fluvial systems (Fig. 14c). Our detrital thermochronology results emphasize the importance of sediment recycling of the Cretaceous foredeep strata, heterogeneous sediment provenance and persistence of rapidly cooled volcanogenic sediments.

The combined U–Pb and He dating of zircon from the Patagonian Magallanes basin reveals that burial of basin sediments and subsequent exhumation and erosional recycling of this sediment into younger strata were important processes throughout the Cenozoic era.

The Middle Miocene basin record indicates a pronounced resurgence of the Cretaceous and Jurassic zircon populations, similar in distribution and relative magnitude to those measured in the upper Dorotea Formation (Fig. 6). This reappearance may be attributed to uplift and recycling of sediment derived from the Upper Cretaceous foredeep via thrusting and/or rejuvenated fluvial connectivity to the batholith sources (Fig. 14c). Our results and thermal modelling lead us to favour the interpretation that these pre-Cenozoic zircons were predominantly recycled from the nearby Upper Cretaceous–Palaeocene foreland strata that were deeply buried and now exposed in the thrust belt.

The model results (Figs 11 and 12) and our interpretations of them do not preclude the possibility of an additional direct source from the Jurassic and Cretaceous magmatic arcs to explain the observed Eocene He dates (Fig. 7). In fact, the existence of detrital zircons with nearly concordant U–Pb and He dates in the Cenozoic samples (Fig. 7), in conjunction with abundant volcanic lithic clasts, provides compelling evidence of continued direct sedimentary transport from the Cenozoic magmatic arc to the Magallanes basin. For the Mesozoic zircon component in Cenozoic deposits, however, we favour a recycled thrust belt provenance rather than a direct contribution from the Mesozoic plutons themselves. This notion is based on the similarity in thermal histories for both the Cretaceous strata and Mesozoic sediment in the Middle Miocene deposits. Although regional denudation can produce uniform age distributions (e.g. Lovera *et al.*, 1999), it seems unlikely that our results can be explained by regional denudation patterns within the Patagonia Batholith. This interpretation is consistent with independent geologic evidence for Early Miocene structural uplift and unroofing of the Cretaceous foredeep from >5 km depth (Harambour, 2002; Fosdick *et al.*, 2011a, 2013). Although the batholith continued to be a source of detritus to the foreland basin until at least *ca.* 14 Ma, the similar thermal histories for the pre-Cenozoic zircons support an interpretation in which grains shared a common Palaeogene burial heating history (Fig. 13).

In contrast to the stable sediment dispersal system in the Late Cretaceous axial foredeep, the detrital zircon record from proximal Oligocene–Miocene foreland basin strata show along-strike heterogeneity in sediment sources. We interpret many of the Palaeogene zircons (29–45 Ma) with nearly overlapping He dates in these younger strata to be derived from the Palaeogene magmatic arc and its volcanic carapace that blanketed the orogen and have since been eroded (Fig. 14c). Active arc magmatism during this time would have elevated the regional Palaeogene heat flow. Upsection, detrital geochronology from the Santa Cruz Formation shows variable zircon U–Pb age distributions, indicating an active volcanic source in the north (Río Baguales area) and a larger component of recycled thrust belt and Palaeogene arc sources in the south (Cordillera Chica area). These signatures are consistent with development of a transverse drainage pattern during the Middle Miocene evolution of the Patagonian Andes.

Presently, the retroarc foreland basin is geographically isolated from the Mesozoic batholith by the Tobífera thrust sheets in the Patagonian thrust belt (Fig. 2). Based on the presence of Palaeogene volcanic zircons in the Middle Miocene sediments, we suggest that east-flowing rivers drained the topographically high Palaeogene arc and traversed large regions of the thrust belt (Fig. 14c). It follows that the modern drainage divide (located *ca.* 100 km east of the Palaeogene arc) was established sometime after deposition of the *ca.* 19-18 Ma Santa Cruz Formation. The timing of thrust belt widening and corresponding eastward shift in the drainage contrasts with events in the Fuegian Andes, where an abrupt reduction in batholith-derived zircons and a change in heavy mineral assemblage are interpreted to reflect much earlier isolation of the Magallanes basin from the batholith in Late Eocene time (Barbeau *et al.*, 2009; Zahid & Barbeau, 2010). Taken together, these detrital records suggest diachronous northward progression of thrust belt widening and migration of the drainage divide across Tierra del Fuego and the southern Patagonian Andes.

CONCLUSIONS

Combined detrital zircon U–Pb geochronology and He thermochronology from the Maastrichtian–Middle Miocene Patagonian Magallanes basin demonstrate that sediment was derived from the Patagonian batholith and recycled Upper Cretaceous strata in the Patagonian thrust belt. Rapidly cooled Palaeocene–Eocene zircons confirm continued connectivity to the magmatic arc during Cenozoic foreland sedimentation. Forward modelling of He dates from prescribed thermal histories for Mesozoic grains suggests extensive post-depositional heating of the Maastrichtian Dorotea Formation to *ca.* 164–180 °C

between 54 and 45 Ma. In the light of best-fit thermal modelling results, we hypothesize that such heating was caused by continued high rates of basin subsidence and sediment supply, leading to stratigraphic burial during Palaeogene time. Moreover, the attenuated Patagonian lithosphere was further weakened by Eocene magmatism, which likely led to elevated temperatures in the subsiding foreland basin. These findings shed light on an important time interval when the Patagonian foreland basin record is represented by a *ca*. 25 Myr unconformity across the foreland.

Thermal modelling of Mesozoic zircons in the Middle Miocene Santa Cruz Formation suggests that these sediments experienced similar thermal histories to those of the Upper Cretaceous deposits. Based upon deformation the exhumation record of the Patagonian thrust belt and our analysis of information regarding the denudation history of the Patagonian batholith, we suggest that Middle Miocene sediments were most likely derived from recycling of deeply buried Upper Cretaceous strata in the Patagonian thrust belt. Additional detritus was derived from the Cenozoic magmatic arc. The interpretations for the Middle Miocene Patagonian Magallanes basin and its complex sediment provenance demonstrate the added value provided by thermal history data for discriminating between different dispersal interpretations compared to having sediment age information alone. Our thermal modelling approach offers insight into the effects of burial heating on thermochronology data and constraints for testing plausible geologic scenarios in tectonically active foreland basins.

ACKNOWLEDGEMENTS

The authors thank Andrea Fildani, Anne Bernhardt, George Hilley, Theresa Schwartz, Jacob Covault, Lisa Stright, Matthew Malkowski and Enrique Bostelmann for invigorating discussions about the Magallanes Basin. U–Pb analytical assistance was provided by personnel at the University of Arizona LaserChron Center. Matthew Coble, Trevor Dumitru, Samuel Johnstone, Melanie Michalak and Guangsheng Zhuang provided assistance in the noble gas laboratories at Stanford University and UC Santa Cruz. We gratefully acknowledge funding from the Stanford School of Earth Sciences, AAPG Grant-in-Aid Program, GSA Student Research Grant Program and the Industry Sponsors of the Stanford Project on Deep-water Depositional Systems. Thoughtful reviews by Richard Ketcham, Jeffrey Rahl, Editor Peter van der Beek and an anonymous reviewer greatly improved the clarity and scope of this work.

SUPPORTING INFORMATION

Additional Supporting Information may be found in the online version of this article:

Table S1. Sample location information for detrital zircon thermochronology samples.

Table S2. Detrital zircon U–Pb geochronologic analyses by LA-ICP-MS analysis. The * indicates radiogenic Pb (corrected for common Pb). All errors are reported at the 1σ level.

Table S3. Combined zircon U–Pb and He data from subset of selected detrital zircons. *Ft* is the alpha-ejection correction after Farley (2002). Samples in italics indicate discordant grains that are not included in probability distribution calculations.

Table S4. Thermal modelling input parameters for calculating forward modelled He dates.

Table S5. Parameters used for decompacted sedimentation and erosion rates.

Figure S1. Tera-Wasserburg Concordia diagrams for zircon U–Pb data. All plots were made with Isoplot (Ludwig, 2008).

Figure S2. Cumulative probability distributions for modelled zircon He dates calculated from best-fit thermal histories. Best-fit distributions are shown for thermal models that pass the Kolmogorov–Smirnoff statistical test (K–S) with probability values >0.68 and >0.95 compared to measured cumulative distribution of He dates (black line). Top: Maastrichtian Dorotea Formation (samples 09-208 and 09-226). Bottom: Miocene Santa Cruz Formation (for > 65 Ma grains from samples 09-235 and 09-207). See text for details.

REFERENCES

Allen, R.B. (1982) Geología de la Cordillera Sarmiento, Andes Patagónicos, entre los 50°00′ S y 52°15′ S, Magallanes, Chile. *Servicio Nacional de Geologia y Mineria, Chile, Boletin*, **38**, 1–46.

Armitage, D.A., Romans, B.W., Covault, J.A. & Graham, S.A. (2009) The influence of mass transport deposit surface topography on the evolution of turbidite architecture: the Sierra Contreras, Tres Pasos Formation (Cretaceous), southern Chile. *J. Sediment. Res.*, **79**, 287–301.

Barbeau, D.L., Olivero, E.B., Swanson-Hysell, N.L., Zahid, K.M., Murray, K.E. & Gehrels, G.E. (2009) Detrital zircon geochronology of the eastern Magallanes foreland basin: implications for Eocene kinematics of the northern Scotia Arc and Drake Passage. *Earth Planet. Sci. Lett.*, **20**, 23–45.

Bernhardt, A., Jobe, Z., Grove, M. & Lowe, D. (2011) Palaeogeography and diachronous infill of an ancient deep-marine foreland basin, Upper Cretaceous Cerro Toro Formation, Magallanes basin. *Basin Res.* doi.10.1111/j.1365-2117.2011.00528.x.

Biddle, K.T., Uliana, M.A., Mitchum, R.M., Jr, Fitzgerald, M.G. & Wright, R.C. (1986) The stratigraphic and structural evolution of the central and eastern Magallanes basin, southern South America. In: *Foreland Basins* (Ed. by Allen P.A. & Homewood P.), *Int. Assoc. Sedimentol. Spec. Publ.*, pp. 41–63. Blackwell Scientific Publications, Oxford.

Blisniuk, P.M., Stern, L.A., Chamberlain, C.P., Idleman, B. & Zeitler, P.K. (2005) Climate and ecological changes during Miocene surface uplift in the southern Patagonian Andes. *Earth Planet. Sci. Lett.*, **230**, 125–142.

Bostelmann, J.E., Le Roux, J.P., Vásquez, A., Gutiérrez, N.M., Oyarzún, J.L., Carreño, C., Torres, T., Otero, R., Llanos, A., Fanning, C.M. & Hervé, F. (2013) Burdigalian deposits of the Santa Cruz Formation in the Sierra Baguales, Austral (Magallanes) Basin: Age, depositional environment and vertebrate fossils. *Andean Geol.*, **40**, 459–489.

Calderón, M., Fildani, A., Hervé, F., Fanning, C.M., Weislogel, A. & Cordani, U. (2007) Late Jurassic bimodal magmatism in the northern sea-floor remnant of the Rocas Verdes basin, southern Patagonian Andes. *J. Geol. Soc.*, **162**, 1011–1022.

Calderón, M., Fosdick, J.C., Warren, C., Massonne, H.-J., Fanning, C.M., Cury, L.F., Schwanethal, J., Fonseca, P.E., Galaz, G., Gaytán, D. & Hervé, F. (2012) The low-grade Canal de las Montañas Shear Zone and its role in the tectonic emplacement of the Sarmiento Ophiolitic Complex and Late Cretaceous Patagonian Andes orogeny, Chile. *Tectonophysics*, **524**, 165–185.

Cherniak, D.J., Watson, E.B. & Thomas, J.B. (2009) Diffusion of helium in zircon and apatite. *Chem. Geol.*, **268**, 155–166.

Ghiglione, M.C. & Ramos, V.A. (2005) Progression of deformation and sedimentation in the southernmost Andes. *Tectonophysics*, **405**, 25–46.

Cina, S.E., Yin, A., Grove, M., Dubey, C.S., Shukla, D.P., Lovera, O.M., Kelty, T.K., Gehrels, G.E. & Foster, D.A. (2009) Gangdese arc detritus within the eastern Himalayan Neogene foreland basin: implications for the Neogene evolution of the Yalu-Brahmaputra River system. *Earth Planet. Sci. Lett.*, **285**, 150–162.

Covault, J.A., Romans, B.W. & Graham, S.A. (2009) Outcrop expression of a continental-margin-scale shelf-edge delta from the Cretaceous Magallanes basin, Chile. *J. Sediment. Res.*, **79**, 523–539.

Crane, W.H. & Lowe, D.R. (2008) Architecture and evolution of the Paine channel complex, Cerro Toro Formation (Upper Cretaceous), Silla Syncline, Magallanes basin, Chile. *Sedimentology*, **55**, 979–1009.

Cuitiño, R.I. & Scasso, R.A. (2010) Sedimentología y paleoambientes del Patagoniano y su transición a La Formación Santa Cruz al sur del Lago Argentino, Patagonia Austral. *Revista de la Asociación Geológica Argentina*, **66**, 406–417.

Cuitiño, J.I., Pimentel, M.M., Santos, M.V. & Scasso, R.A. (2012) High Resolution Isotopic Ages for the Early Miocene 'Patagoniense' Transgression in Southwest Patagonia. Stratigraphic Implications. *J. S. Am. Earth Sci.*, **38**, 110–122.

Dalziel, I.W.D. (1986) Collision and Cordilleran orogenesis: an Andean perspective. In: *Collision Tectonics* (Ed. by Coward M.P. & Reis A.C.), *Geol. Soc. Spec. Pub.*, **19**, 389–404.

Dalziel, I.W.D., de Wit, M.J. & Palmer, K.F. (1974) Fossil marginal basin in the southern Andes. *Nature*, **250**, 291–294.

Degraaff-Surpless, K., Graham, S.A., Wooden, J.L. & McWilliams, M.O. (2002) Detrital zircon provenance analysis of the Great Valley Group, California: evolution of an arc-forearc system. *Geol. Soc. Am. Bull.*, **114**, 1564–1580.

Dickinson, W.R. (1988) Provenance and sediment dispersal in relation to paleotectonics and paleogeography of sedimentary basins. In: *New Perspectives in Basin Analysis* (Ed. by K.L. Kleinspehn, C. Paola), pp. 3–25. Springer, New York.

Dickinson, W.R. & Suczek, C.A. (1979) Plate tectonics and sandstone compositions. *Am. Assoc. Pet. Geol. Bull.*, **63**, 2164–2182.

Ehlers, T.A. (2005) Crustal thermal processes and the interpretation of thermochronometer data. *Rev. Mineral. Geochem.*, **58**, 315–350.

Einsele, G., Ratschbacher, L. & Wetzel, A. (1996) The Himalaya-Bengal Fan denudation-accumulation system during the past 20 Ma. *J. Geol.*, **104**, 163–184.

Farley, K.A. (2002) (U-Th)/He dating: techniques, Calibrations and applications. *Rev. Min. Geochem.*, **47**, 819–844.

Fildani, A. & Hessler, A.M. (2005) Stratigraphic record across a retroarc basin inversion: Rocas Verdes – Magallanes basin, Patagonian Andes. *Geol. Soc. Am. Bull.*, **117**, 1596–1614.

Fildani, A., Cope, T.D., Graham, S.A. & Wooden, J.L. (2003) Initiation of the Magallanes foreland basin: timing of the southernmost Patagonian Andes orogeny revised by detrital zircon provenance analysis. *Geology*, **31**, 1081–1084.

Flowers, R.M., Ketcham, R.A., Shuster, D.L. & Farley, K.A. (2009) Apatite (U-Th)/He thermochronometry using a radiation damage accumulation and annealing model. *Geochim. Cosmochim. Acta*, **73**, 2347–2365.

Forsythe, R. & Allen, R.B. (1980) The basement rocks of PenÍnsula Staines, Región XII, Province of Última Esperanza, Chile. *Revista Geológica de Chile*, **10**, 3–15.

Fosdick, J.C. & Carrapa, B. (2012) Paleogene initiation of Andean foreland sedimentation in the Bermejo Basin and Precordillera thrust belt of NW Argentina from detrital geochronology and thermochronology. *Geol. Soc. Am. Abstracts with Programs*, **44**, 72.

Fosdick, J.C., Romans, B.W., Fildani, A., Calderón, M.N., Bernhardt, A. & Graham, S.A. (2011a) Kinematic history of the Cretaceous-Neogene Patagonia thrust belt and Magallanes foreland Basin, Chile and Argentina (51°30' S). *Geol. Soc. Am. Bull.*, **123**, 1679–1698.

Fosdick, J.C., Hilley, G.E. & Graham, S.A. (2011b) Flexural analysis of the Magallanes retroarc basin of southern South America: A 1-D elastic-plastic model for deflection of attenuated lithosphere. American Geophysical Union, Fall Meeting, abstract #T11B-2334.

Fosdick, J.C., Grove, M., Hourigan, J.K. & Calderón, M. (2013) Retroarc deformation and exhumation near the end of the Andes, southern Patagonia. *Earth Planet. Sci. Lett.*, **361**, 504–517.

Furque, G. (1973) Descripción geológica de la Hoja 58b Lago Argentino. *Boletin del Servicio Nacional Minero y Geológico*, **140**, 1–49.

Galaz, G., Hervé, F. & Calderón, M. (2005) Metamorfismo y deformación de la Formacion Tobífera en la cordillera Riesco, región de Magallanes Chile: evidencias para su evolución tectónica. *Revista de la Asociación Geológica Argentina*, **60**, 1–18.

Gehrels, G.E., Valencia, V. & Pullen, A. (2006) Detrital zircon geochronology by Laser-Ablation Multicollector ICPMS at the Arizona LaserChron Center. In:*Geochronology: Emerging Opportunities, Paleontology Society Short Course* (Ed. by Loszewski T. & Huff W.), *Paleontology Society Papers*, **11**, 10.

Gombosi, D.L., Barbeau, D.L., Jr. & Garver, J.I. (2009) New thermochronometric Constraints on the rapid Paleogene exhumation of the Cordillera Darwin Complex and related thrust sheets in the Fuegian Andes. *Terra Nova*, **21**, 507–515.

Graham, S.A., Tolson, R.B., Decelles, P.G., Ingersoll, R.V., Bargar, E., Caldwell, M., Cavazza, W., Edwards, D.P., Follo, W.F., Handschy, J.W., Lemke, L., Moxon, I., Rice, R., Smith, G.A. & White, J. (1986) Provenance modelling as a technique for analysing source terrane evolution and controls on foreland sedimentation. *Special Publication of the International Association of Sedimentologists*, **8**, 425–436.

Graham, S.A., Hendrix, M.S., Wang, L.B. & Carroll, A.R. (1993) Collisional successor basins of western China; impact of tectonic inheritance on sand composition. *Geol. Soc. Am. Bull.*, **105**, 323–344.

Guenthner, W.R., Reiners, P.W., Ketcham, R.A., Nasdala, L. & Giester, G. (2013) Helium diffusion in natural zircon: radiation damage, anisotropy, and the interpretation of zircon (U-Th)/He thermochronology. *Am. J. Sci.*, **313**, 1456–198.

Hamza, V.M. & Muñoz, M. (1996) Heat Flow Map of South America. *Geothermics*, **25**, 599–621.

Harambour, S.M. (2002) Deep-seated Thrusts in the Frontal Part of the Magallanes Fold and Thrust Belt, Ultima Esperanza, Chile. *15th Congreso Geológico Argentino Actas*, **3**, 232.

Heller, P.L. & Frost, C.D. (1988) Isotopic provenance of clastic deposits–application of geochemistry to sedimentary provenance studies. In: *New Perspectives in Basin Analysis* (Ed. by K. Kleinspehn & C. Paola), pp. 27–42. Springer-Verlag, New York.

Hervé, F., Fanning, C.M. & Pankhurst, R.J. (2003) Detrital zircon age patterns and provenance of the metamorphic complexes of southern Chile. *J. S. Am. Earth Sci.*, **16**, 107–123.

Hervé, F., Godoy, E., Mpodozis, C. & Fanning, M. (2004) Monitoring magmatism of the Patagonian Batholith through the U-Pb SHRIMP dating of detrital zircons in sedimentary units of the Magallanes basin. *Bolletino di Geofísica Teorica ed Applicata*, **45**, 113–117.

Hervé, F., Massonne, H.-J., Calderón, M. & Theye, T. (2007a) Metamorphic P-T conditions of Late Jurassic rhyolites in the Magallanes fold and thrust belt, Patagonian Andes, Chile. *J. Iberian Geol.*, **33**, 5–16.

Hervé, F., Pankhurst, R.J., Fanning, C.M., Calderón, M. & Yaxley, G.M. (2007b) The South Patagonian batholith: 150 my of granite magmatism on a plate margin. *Lithos*, **97**, 373–394.

Hofftstetter, R., Fuenzalida, H. & Cecioni, G. (1957) Lexique Stratigraphique International., v. V, Amérique Latine, Fascicule 7, Chile. Centre Nacional de la Recherche Scientifique, Paris, 444 pp.

Hourigan, J.K., Reiners, P.W. & Brandon, M.T. (2005) U-Th zonation dependent alpha-ejection correction in (U-Th)/He chronometry. *Part I: Theory: Geochimica et Cosmochimica Acta*, **69**, 3349–3365.

Hubbard, S.M., Romans, B.W. & Graham, S.A. (2008) Deep-water foreland basin deposits of the Cerro Toro Formation, Magallanes basin, Chile: architectural elements of a sinuous basin axial channel belt. *Sedimentology*, **55**, 1365–3091.

Hünicken, M. (1955) Depósitos neocretácios y terciario s del extreme SSW de Santa Cruz. Cuenca carbonífera de Río Turbio. Revista del Instituto Nacional de Investigaciones de las Ciencas Naturales y Museo Argentino de Ciencias Naturales "Bernardino Rivadavia". *Ciencias Geológicas*, **4**, 1–164.

Katz, H.R. (1963) Revision of Cretaceous stratigraphy in Patagonian cordillera of Ultima Esperanza, Magallanes Province, Chile. *AAPG Bull.*, **47**, 506–524.

Kay, S.M., Ramos, V.A. & Gorring, M.L. (2002) Geochemistry of Eocene plateau basalts related to ridge collision in southern Patagonia. *XV Congreso Geológico Argentino*, **3**, 60–65.

Ketcham, R.A. (2005) Forward and inverse modeling of low-temperature thermochronometry data. *Rev. Mineral. Geochem.*, **58**, 275–314.

Ketcham, R.A., Guenthner, W.R. & Reiners, P.W. (2013) Geometric analysis of radiation damage connectivity in zircon and its implications for helium diffusion. *Am. Mineral.*, **98**, 350–360.

Klepeis, K., Betka, P., Clarke, G., Fanning, M., Hervé, F., Rojas, L., Mpodozis, C. & Thomson, S. (2010) Continental underthrusting and obduction during the Cretaceous closure of the Rocas Verdes rift basin, Cordillera Darwin, Patagonian Andes. *Tectonics*, **29**, TC3014.

Kohn, M.J., Spear, F.S. & Dalziel, I.W.D. (1993) Metamorphic P-T Paths from Cordillera Darwin, a core complex in Tierra del Fuego, Chile. *J. Petrol.*, **34**, 519–542.

Kraemer, P.E. (1998) Structure of the Patagonian Andes: regional balanced cross section at 50°S, Argentina. *Int. Geol. Rev.*, **40**, 896–915.

Le Roux, J.P., Puratich, J., Mourgues, A., Oyarzún, J.L., Otero, R.A., Torres, T. & Hervé, F. (2010) Estuary deposits in the Río Baguales Formation (Chattian-Aquitanean), Magallanes Province, Chile. *Andean Geology*, **37**, 329–344.

Lovera, O.M., Richter, F.M. & Harrison, T.M. (1989) The $^{40}Ar/^{39}Ar$ geothermometry for slowly cooled samples having a distribution of diffusion domain sizes. *J. Geophys. Res.*, **94**, 17917–17935.

Lovera, O.M., Grove, M., Kimbrough, D.L. & Abbott, P.L. (1999) A method for evaluating basement exhumation histories from closure age distributions of detrital minerals. *J. Geophys. Res.*, **104**, 29,419-29,438.

Ludwig, K.R. (2008) Isoplot 3.6: Berkeley Geochronology Center, Special Publication, 4, 77.

Macellari, C.E., Barrio, C.A. & Manassero, M.J. (1989) Upper Cretaceous to Paleocene depositional sequences and sandstone petrography of south-western Patagonia (Argentina and Chile). *J. S. Am. Earth Sci.*, **2**, 223–239.

Malumián, N. & Caramés, A. (1997) Upper Campanian-Paleogene from the Río Turbio coal measures in southern Argentina: micropaleontology and the Paleocene/Eocene boundary. *J. S. Am. Earth Sci.*, **10**, 189–201.

Malumián, N. & Náñez, C. (1988) El género Transversigerina y la edad de la transgression Patagoniana. 6° Congreso Nacional de Geología Económica Actas, 1, 285–290.

Malumián, N., Panza, J.L., Parisi, C., Nanez, C., Caramés, A. & Torre, A. (2000) Hoja Geológica 5172-III, Yacimiento Río Turbio (1:250,000). *Servicio Geologico Minero Argentino, Boletin*, **247**, 180, Buenos Aires.

Mcdougall, I. & Harrison, T.M. (1999) *Geochronology and Thermochronology by the $^{40}Ar/^{39}Ar$ Method*, 2nd edn. Oxford University Press, Oxford.

McAtamney, J., Klepeis, K., Mehrtens, C., Thomson, S.N., Betka, P., Rojas, L. & Snyder, S. (2011) Along-strike variability of back-arc basin collapse and the initiation of sedimentation in the Magallanes foreland basin, southernmost Andes (53–54.5°S). *Tectonics*, **30**, 1–26.

Natland, M.L., Gonzalez, P.E., Canon, A. & Ernst, M. (1974) A system of stages for correlation of Magallanes basin sediments. *Am. Assoc. Pet. Geol. Mem.*, **139**, 126.

Nullo, F.E., Proserpio, C.A. & Blasco de Nullo, G. (1981) El Cretacico de la Cuenca Austral entre el Lago San Martin y

RioTurbio. In: *Cuencas Sedimentarias del durasico y Cretacico de America del Sur, 1* (Ed. by W. Volkeimer & E.A. Musacchio), pp. 181–220. ComitÉ Sudamericano del JurÁsico y CretÁcico, Buenos Aires.

Nullo, F.E., Haller, M.J., Panza, J.L., Marin, G. & Pardo, M.I. (1993) Basaltos alcalinos eocenos y miocenos de algunas localidades de la Patagonia (Chubut y Santa Cruz). *Revista Asociación Geológica Argentina*, **48**, 23–49.

Otero, R.A., Torres, T., le Roux, J.P., Hervé, F., Fanning., C.M., Yury-Yáñez, R.E. & Rubilar-Rogers, D. (2012) A Late Eocene age proposal for the Loreto Formation (Brunswick Peninsula, southernmost Chile), based on fossil cartilaginous fishes, paleobotany and radiometric evidence. *Andean Geology*, **39**, 180–200.

Pankhurst, R.J., Riley, T.R., Fanning, C.M. & Kelley, S.P. (2000) Episodic silicic volcanism in Patagonia and Antarctic Peninsula: chronology of magmatism associated with the break-up of Gondwana. *J. Petrol.*, **41**, 605–625.

Pankhurst, R.J., Rapela, C.W., Loske, W.P., Fanning, C.M. & Márquez, M. (2003) Chronological study of the pre-Permian basement rocks of southern Patagonia. *J. S. Am. Earth Sci.*, **16**, 27–44.

Pankhurst, R.J., Rapela, C.W., Fanning, C.M. & Márquez, M. (2006) Gondwanide continental collision and the origin of Patagonia. *Earth-Sci. Rev.*, **76**, 235–257.

Pearson, N.J., Mángano, M.G., Buatois, L.A., Casadío, S. & Raising, R.M. (2012) Ichnology, sedimentology, and sequence stratigraphy of outer-estuarine and coastal-plain deposits: Implications for the distinction between allogenic and autogenic expressions of the Glossifungites Ichnofacies. *Palaeogeogr. Palaeoclimatol. Palaeoecol.*, **333**, 192–217.

Press, S.J. (1989) *Bayesian Statistics: Principles, Models, and Applications*. John Wiley and Sons, New York.

Rahl, J.M., Reiners, P.W., Campbell, I.H., Nicolescu, S. & Allen, C.M. (2003) Combined single-grain (U-Th)/He and U-Pb dating of detrital zircons from the Navajo Sandstone, Utah. *Geology*, **31**, 761–764.

Ramírez de Arellano, C., Putlitz, B., Müntener, O. & Ovtcharova, M. (2012) High precision U/Pb zircon dating of the Chaltén Plutonic Complex (Cerro Fitz Roy, Patagonia) and its relationship to arc migration in the southernmost Andes. *Tectonics*, **31**. doi:10.1029/2011TC003048.

Ramos, V.A. & Kay, S.M. (2002) Southern Patagonian plateau basalts and deformation: backarc testimony to ridge collisions. *Tectonophysics*, **205**, 261–282.

Reiners, P.W. & Brandon, M.T. (2006) Using thermochronology to understand orogenic erosion, Annu. *Rev. Earth Planet. Sci.*, **34**, 419–466.

Reiners, P.W. & Nicolescu, S. (2006) Measurement of parent nuclides for (U-Th)/He chronometry by solution sector ICP-MS, *ARHDL Report 1*, http://www.geo.arizona.edu/~reiners/arhdl/arhdl.htm

Reiners, P.W., Spell, T.L., Nicolescu, S. & Zanetti, K.A. (2004) Zircon (U-Th)/He thermochronometry: he diffusion and comparisons with 40Ar/39Ar dating. *Geochim. Cosmochim. Acta*, **68**, 1857–1887.

Reiners, P.W., Campbell, I.H., Nicolescu, S., Allen, C.A., Hourigan, J.K., Garver, J.I., Mattinson, J.M. & Cowan, D.S. (2005) (U-Th)/(He-Pb) "double-dating" of detrital zircons. *Am. J. Sci.*, **305**, 259–311.

Riccardi, A.C. & Rolleri, E.O. (1980) Cordillera PatagÓnica Austral. *Actas Segundo Simposio de GeologÍa Regional Argentina*, **2**, 1173–1306.

Romans, B.W., Fildani, A., Graham, S.A., Hubbard, S.M. & Covault, J.A. (2010) Importance of predecessor basin history on sedimentary fill of a retroarc foreland basin: provenance analysis of the Cretaceous Magallanes basin, Chile (50°52'S). *Basin Res.*, **22**, 640–658.

Romans, B.W., Hubbard, S.M. & Graham, S.A. (2009) Stratigraphic evolution of an outcropping continental slope system, Tres Pasos Formation at Cerro Divisadero, Chile. *Sedimentology*, **56**, 737–764.

Romans, B.W., Fildani, A., Hubbard, S.M., Covault, J.A., Fosdick, J.C. & Graham, S.A. (2011) Evolution of deep-water stratigraphic architecture, Magallanes basin, Chile. *Mar. Pet. Geol.* doi: 10.1016/j.marpetgeo.2010.05.002.

Russo, A., Flores, M.A. & di Benedetto, H. (1980) Patagonia Austral Extraandina. *Segundo Simposio de Geología Regional Argentina Actas*, **2**, 1431–1462.

Saylor, J.E., Stockli, D.F., Horton, B.K., Nie, J. & Mora, A. (2012) Discriminating rapid exhumation from syndepositional volcanism using detrital zircon double dating: implications for the tectonic history of the eastern Cordillera, Colombia. *Geol. Soc. Am. Bull.*, **124**, 762–779.

Schmitt, J.G. & Steidtmann, J.R. (1990) Interior ramp-supported uplifts: implications for sediment provenance in foreland basins. *Geol. Soc. Am. Bull.*, **102**, 494–501.

Schwartz, T., Malkowski, M. & Graham, S.A. (2012) Evaluation of the Close-Out of Deep-Marine Deposition in the Magallanes/Austral Basin, Patagonian Chile and Argentina. AAPG Search and Discovery Article #90142.

Scott, K.M. (1966) Sedimentology and dispersal patterns of a Cretaceous flysch sequence, Patagonian Andes, southern Chile. *Am. Assoc. Pet. Geol. Bull.*, **50**, 72–107.

Shuster, D.L., Flowers, R.M. & Farley, K.A. (2006) The influence of natural radiation damage on helium diffusion kinetics in apatite. *Earth Planet. Sci. Lett.*, **249**, 148–161.

Skarmeta, J.J. & Castelli, J.C. (1997) Syntectonic intrusion of the Torres del Paine granite, Patagonian Andes. *Chile. Rev. Geol. Chile*, **24**, 55–74.

Steidtmann, J.R. & Schmitt, J.G. (1988) Provenances and dispersal of tectogenic sediments in thin-skinned, thrusted terrains. In: *New Perspectives in Basin Analysis* (Ed. by K. Kleinspehn, C. Paola), pp. 353–366. Springer, Berlin.

Suttner, L.J. (1974) Sedimentary petrographic provinces – An evaluation. *SEPM Spec. Publ.*, **20**, 75–84.

Thomson, S.N., Hervé, F. & Stockhert, B. (2001) The Mesozoic-Cenozoic denudation history of the Patagonian Andes (southern Chile) and its correlation to different subduction processes. *Tectonics*, **20**, 693–711.

Thomson, S.N., Brandon, M.T., Reiners, P.W., Tomkin, J.H., Vásquez, C. & Wilson, N.J. (2010) Glaciation as a destructive and constructive control on mountain building. *Nature*, **467**, 313–317.

Waschbusch, P.J. & Royden, L.H. (1992) Spatial and temporal evolution of foredeep basins: lateral strength variations and inelastic yielding in continental lithosphere. *Basin Res.*, **4**, 179–195.

Wilson, T.J. (1983) Stratigraphic and structural evolution of the Ultima Esperanza foreland fold-thrust belt, Patagonian Andes, Southern Chile *[Ph.D. thesis]*. Columbia University, New York.

Wilson, T.J. (1991) Transition from back-arc to foreland basin development in southernmost Andes: stratigraphic record

from the Ultima Esperanza District, Chile. *Geol. Soc. Am. Bull.*, **103**, 98–111.

Winn, R.D., Jr. & Dott, R.H., Jr. (1979) Deep-water fan-channel conglomerates of late Cretaceous age, southern Chile. *Sedimentology*, **26**, 203–228.

Wolf, R.A., Farley, K.A. & Silver, L.T. (1996) Helium diffusion and low-temperature thermochronometry of apatite. *Geochim. Cosmochim. Acta*, **60**, 4231–4240.

Yrigoyen, M. (1969) Problemas estratigráficos del Terciano de Argentina. *Ameghiniana*, **6**, 315–329.

Zahid, K.M. & Barbeau, D.L. (2010) Provenance of eastern magallanes foreland basin sediments: heavy mineral analysis reveals paleogene tectonic unroofing of the fuegian Andes Hinterland. *Sed. Geol.*, **229**, 64–74.

Zeitler, P.K., Herczeg, A.L., McDougall, I. & Honda, M. (1987) U-Th-He dating of apatite; a potential thermochronometer. *Geochim. Cosmochim. Acta*, **51**, 2865–2868.

Manuscript received 08 November 2013; In revised form 17 July 2014; Manuscript accepted 20 July 2014.